Experimental and Theoretical Work on Reverse Osmosis - Dual Stage Pressure Retarded Osmosis Hybrid System

Nahawand Al-Zainati[1], Senthilmurugan Subbiah[2], Sudesh Yadav[1], Ali Altaee[1*], Pietro Bartocci[4,5], Ibrar Ibrar[1], John Zhou[1], Akshaya K. Samal[3], Francesco Fantozzi[4]

1: Centre for Green Technology, School of Civil and Environmental Engineering, University of Technology Sydney, 15 Broadway, NSW, 2007, Australia

2: Department of Chemical Engineering, Indian Institute of Technology Guwahati, Guwahati, Assam -781039, India

3: Centre for Nano and Material Sciences, Jain University, Jain Global Campus, Ramanagara, Bangalore 562112, India

4: Department of Engineering, University of Perugia, Via G. Durante 67, Perugia 06125, Italy

5: Instituto de Carboquímica (C.S.I.C.), Miguel Luesma Castán 4, 50018 Zaragoza, Spain

*Corresponding author email: Ali.altaee@uts.edu.au

Abstract

Two-pass reverse osmosis desalination is a common process to treat high-salinity feed solution and provides a low-salinity permeate solution. This study investigated the significance of the energy generated by the dual-stage pressure retarded osmosis (DSPRO) from the reverse osmosis (RO) brine stream. The main components of the DSPRO-RO hybrid system are RO, pressure retarded osmosis (PRO), and energy recovery device, and their models are determined. Dymola software, using Modelica modelling language, was utilized for solving the hybrid system models. Two different flowsheets were built; the first included a two-pass RO, while the second is a hybrid of a two-pass RO (2RO)-DSPRO system. Seawater salinities of 40 and 45 g/L were the RO feed solution, and 1 g/L tertiary treated wastewater was the feed solution of the DSPRO process. The net specific energy consumption was calculated for the 2RO and 2RO-DSPRO systems for 40 and 45 g/L salinities. At a 47% recovery rate and 40 g/L seawater salinity, the 2RO-DSPRO system was 14.7% more energy efficient than the 2RO system. The corresponding energy saving at a 47% recovery rate and 45 g/L seawater salinity was 17.5%. The desalination energy for the 2RO system was between 3.25 and 3.49 kWh/m^3, and for the 2RO-DSPRO system was between 2.91 and 2.97 kWh/m^3. The results demonstrate the great potential of integrating the 2RO with the DSPRO to reduce desalination's energy consumption and environmental impacts.

Keywords: Reverse Osmosis (RO), Pressure Retarded Osmosis (PRO), Two-Pass RO-DSPRO, Salinity Gradients, Renewable Energy

Nomenclature

Symbol	Definition
A_{ERD}	The inlets side energy recovery device cross-sectional area in m^2
Am_{RO}	The RO membrane surface area in m^2
Aw_{PRO}	The water permeability of the PRO in m^3/m^2.s.bar
Aw_{RO}	The water permeability of the RO in m^3/m^2.s.bar

B_{PRO}	The salt permeability coefficient of the PRO in m/s
B_{RO}	The salt permeability coefficient of the RO in m/s
$C_{F,RO}$	The feed concentration of the RO in g/L
$C_{Fm,RO}$	The feed membrane side concentration of the RO in g/L
C_{hi}	The high-pressure brine inlet concentration of the ERD in g/L
C_{ho}	The high-pressure feed outlet concentration of the ERD in g/L
$C_{i,e}$ *and* $C_{o,g}$	The inlet and outlet concentration of each stream in the mixer or the splitter in g/L
C_{li}	The low-pressure feed inlet concentration of the ERD in g/L
C_{lo}	The low-pressure brine outlet concentration of the ERD in g/L
$C_{B,RO}$	The brine concentration of the RO in g/L
$C_{p,RO}$	The product (permeate) concentration of the RO in g/L
ρ_{water}	The density of the feed water in ERD in g/m^3
η_{ERD}	The ERD efficiency
η_{Pump}	The pump efficiency
$\eta_{Turbine}$	The turbine efficiency
D_F	The darcy's law constant at the feed side of the RO in bar.s/m^4
DSPRO	Dual Stage Pressure Retarded Osmosis
e and g	The number of inlet and outlet streams in the mixer or the splitter
ERD	Energy recovery device
HPP	High-pressure pump
i	The Van't Hoff factor
J_{RO}	The product water flux of the RO in m/s
K_{FL}	The coefficient of the friction loss in the ERD in m
k_{RO}	The mass transfer coefficient of the RO feed side in m/s
LPP	Low-pressure pump
L_{RO}	The length of the pressure vessel of the RO in m
l_{RO}	The length of the RO membrane module in m
Lub_{flow}	The lubricant flow in the ERD in m^3/h
$Lub_{flowRatio}$	The lubricant flow ratio in the ERD
M	The number of RO membranes in a single pressure vessel
Mwt	The solute molecular weight in g/mol
$\%Mix_{ERD}$	The mixing percentage between the high and the low pressurized streams of the ERD
$P_{Di,PRO}$	The draw inlet pressure of the PRO in bar
$P_{Do,PRO}$	The draw outlet pressure of the PRO in bar
Pd_{RO}	The pressure drop in the RO pressure vessel in bar
$P_{F,RO}$	The feed pressure of the RO in bar
P_{hi}	The high brine inlet pressure of the ERD in bar
P_{ho}	The high feed outlet pressure of the ERD in bar
P_{li}	The low feed inlet pressure of the ERD in bar
P_{lo}	The low brine outlet pressure of the PX in bar
$P_{p,RO}$	The product pressure of the RO in bar
$P_{Pump,H}$	The head pressure of the pump in bar
$P_{Pump,i}$	The pressure of the inlet stream of the pump in bar
$P_{Pump,o}$	The pressure of the outlet stream of the pump in bar
PRO	Pressure Retarded Osmosis
PRO1	The first PRO unit
PRO2	The second PRO unit

$P_{Turbine,i}$	The pressure of the inlet stream of the turbine in bar
$P_{Turbine,o}$	The pressure of the outlet stream of the turbine in bar
PX	Pressure Exchanger
$Q_{B,RO}$	The brine flow rate of the RO in m^3/h
$Q_{Di,PRO}$	The draw inlet flow rate of the PRO in m^3/h
$Q_{Do,PRO}$	The draw outlet flow rate of the PRO in m^3/h
$Q_{F,RO}$	The feed flow rate of the RO in m^3/h
Q_{hi}	The high-pressure brine inlet flow rate of the ERD in m^3/h
Q_{ho}	The high-pressure feed outlet flow rate of the ERD in m^3/h
$Q_{i,e}$ *and* $Q_{o,g}$	The inlet and outlet flow rate of each stream in the mixer or the splitter in m^3/h
Q_{li}	The low-pressure feed inlet flow rate of the ERD in m^3/h
Q_{lo}	The low-pressure brine outlet flow rate of the ERD in m^3/h
$Q_{p,RO}$	The product flow rate of the RO in m^3/h
$Q_{Pump,i}$	The flow rate of the inlet stream of the pump in m^3/h
$Q_{Pump,o}$	The flow rate of the outlet stream of the pump in m^3/s
$Q_{Turbine,i}$	The flow rate of the inlet stream of the turbine in m^3/h
$Q_{Turbine,o}$	The flow rate of the outlet stream of the turbine in m^3/h
R	The universal gas constant in m^3.bar/mol.K
$Recv_{RO}$	The recovery rate of the RO
$Recv_{PRO}$	The recovery rate of the PRO
σ	The reflection coefficient
RO	Reverse Osmosis
$RO1$	The first RO unit
$RO2$	The Second RO unit
S_{PRO}	The membrane structural parameter of the PRO membrane in m
T	Temperature in K
W	The energy generation of the PRO in kW
$W_{Pump,Consumed}$	The energy consumption of the pump in kW
$W_{Turbine}$	The energy generation of the turbine in kW
x_{PRO}, y_{PRO}	Constants in mass transfer coefficient correlation of the PRO
x_{RO}, y_{RO}	Constants in mass transfer coefficient correlation of the RO
ΔP_{RO}	Applied hydraulic pressure difference of the RO in bar
$\Delta\pi_{RO}$	Osmotic Pressure difference of the RO in bar

1. Introduction

Reverse osmosis (RO) has been recognized as the common technology for seawater treatment as the most efficient and affordable technology compared to other desalination processes [1-3]. The theoretical specific energy consumption for seawater desalination is 1.06 kWh/m^3 for seawater of 35 g/L total dissolved solids (TDS) and a 50% recovery rate [4]. For an RO plant with an energy recovery device, the specific power consumption depends on seawater TDS, which is less than 2.0 kWh/m^3 for 35 g/L seawater [5, 6]. Compared to thermal desalination,

RO technology is more energy-efficient and has higher recovery rates [7]. Nevertheless, it is still considered an energy-intensive desalination process, limiting its affordability in countries with high energy prices [8]. There were attempts to reduce the RO energy consumption by coupling it with renewable energy sources such as solar energy [9, 10], geothermal [11, 12], wind energy [13, 14], and wave energy [15, 16]. Integrating the RO plant with renewable energy is constrained by their availability throughout the day; therefore, additional energy sources may be necessary to power the desalination plant. A relatively new type of renewable energy, pressure retarded osmosis (PRO), was suggested for coupling with RO desalination to reduce energy consumption [17-20]. The PRO process is a salinity gradient-operated technology that uses a slightly pressurized RO brine to convert a chemical potential to hydraulic energy [21-23]. The high-pressure RO brine will be pumped into the PRO membrane module for freshwater extraction from a lower salinity feed solution in the RO-PRO hybrid system. The diluted RO brine (the PRO draw solution) will be depressurized in a hydro-turbine system for energy recovery. Previous studies demonstrated that the power consumption of RO desalination could be reduced by 14 to 40% when coupled with the PRO process [24].

Several studies considered coupling the PRO process with the RO desalination plant to reduce energy consumption and brine discharge to the sea. For instance, Altaee et al. [25] investigated the performance of the RO-PRO hybrid system for energy generation. The study underlined the advantage of coupling the RO with the PRO system to reduce the energy consumption of the RO plant by 31%. Results also showed that reducing the draw solution flow rate reduced the RO plant energy consumption. In another study, Quan et al. (2019) [24] investigated the impact of feed temperature on the energy harvested from an RO brine using a PRO unit. The study revealed a 14.41% to 17.93% reduction in the specific energy consumption could be achieved by increasing the PRO operating temperature from 25 ^{o}C to 50 ^{o}C. Moreover, it was noticed that the PRO operating pressure has an inverse relationship with the specific energy consumption of the RO-PRO hybrid system.

Another RO-PRO hybrid study determined the RO recovery rate and feed concentration influence on the PRO membrane area, feed pressure, and draw solution concentration [26]. Using 35 g/L seawater feed solution in the RO plant at a 52% recovery rate produced a maximum power density of 24 W/m^2. However, increasing the seawater salinity to 45 g/L and reducing the recovery rate to 46% increased the PRO power density to 28 W/m^2. The study also reported that adding the PRO system to the RO system caused an 18% increase in the RO recovery rate. He et al. [27] demonstrated that a standalone RO desalination system with an energy recovery device required an optimum net specific energy consumption of around 1.6 kWh/m^3 at a 50% RO recovery rate. At the same recovery rate, coupling the RO desalination system with a PRO unit and energy recovery device caused a 1 kWh/m^3 drop in the optimum net specific energy consumption of the RO plant. The results suggest that adding the PRO system to the RO system could reduce the optimum net specific energy consumption to around 38%.

Touati et al. [28] proposed a hybrid system of two RO units (2RO), an energy recovery device, a pressure exchanger, a turbine, and two PRO units. Each RO membrane unit was coupled individually with a PRO system. The specific energy generation of the first PRO stage at a 50% recovery rate and 80% draw stream dilution was 0.15 kWh/m^3. In the second PRO process operating under the same conditions, the specific energy consumption was 0.57 kWh/m^3. Results also revealed that energy generation had an inverse relationship with the RO recovery

rate. Nevertheless, the study did not include optimization of the specific energy consumption. It should be noted that the 2RO plant is a common design for optimizing the quality of the product water [29]. A dual-stage PRO (DSPRO) process would be suitable for optimizing the performance of the 2RO plant in a fully integrated RO-PRO hybrid system. However, studies that considered the coupling of the DSPRO with the 2RO plant and hybrid system optimization are scarce [28, 30]. In the DSPRO process, the draw solution from the first PRO stage is coupled with a fresh feed solution in the second PRO stage to reduce the concentration polarization effect and improve the harvested energy from the salinity gradient resource [31, 32].

This study evaluated the performance of the 2RO-DSPRO based on the RO specific energy consumption and PRO net specific energy generation as objective functions. Furthermore, model-based optimization will enable the plant for a hybrid 2RO-DSPRO system. Accordingly, this study evaluated the energy efficiency of the 2RO-DSPRO hybrid system (Fig. 1). In the 2RO-DSPRO system, RO1 brine is partially depressurized in the ERD2 before going to the PRO1 for freshwater extraction from the wastewater feed solution. When leaving the PRO1, the diluted draw solution goes to ERD1 to partially pressurize a seawater feed solution. A partially depressurized diluted draw solution will leave ERD1 and enter the PRO2 unit for freshwater extraction from a wastewater feed solution before splitting it into two streams. The first stream goes to a hydro turbine for power generation, and the second stream goes to ERD3 to depressurize the RO1 permeate that forms the RO2 feed solution. The study developed separate models for the RO and PRO processes using the “Modelica” modelling language through the Dymola software. The RO and the PRO models were validated using experimental data. The performance of the 2RO plant was compared with the 2RO-DSPRO plant at different recovery rates and seawater salinities of 40 g/L and 45 g/L. To the best of the authors' knowledge, no study is yet available about the 2RO-DSPRO hybrid system and system optimization to minimize the specific energy consumption of the desalination process.

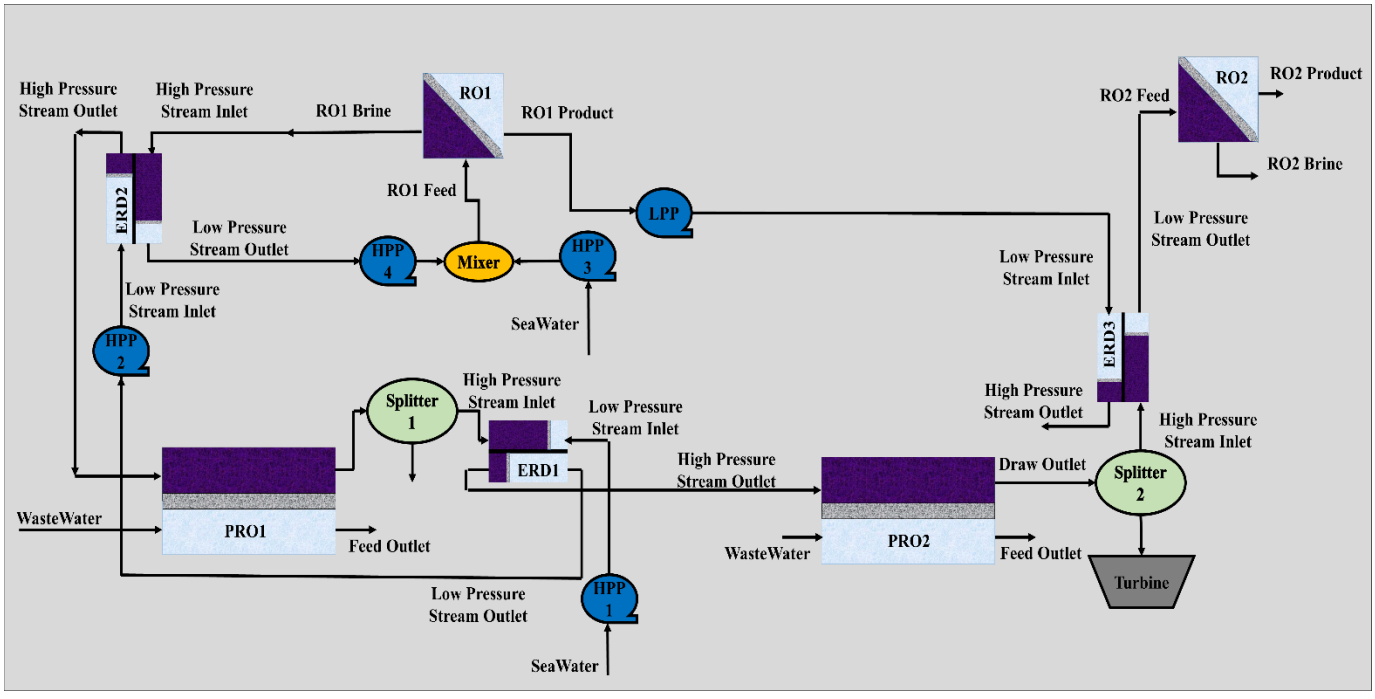

Fig. 1: The 2RO-DSPRO hybrid system

2. Methodology

The hybrid system of the two-pass RO-DSPRO (2RO-DSPRO) includes a turbine, high-pressure pump (HPP), low-pressure pump (LPP), and an energy recovery device (ERD) (Fig. 1). Mathematical models were separately defined in Dymola software for the RO and PRO systems. Accordingly, the other processes' mathematical models will be introduced in this section. The modelling language Modelica is used to model and simulate the RO and the PRO processes by Dymola software and system components such as turbines, pumps, and energy recovery devices. Simulations were performed on the RO and PRO models to determine the applicable range of operating variables.

2.1 The RO Model

The RO process model is developed by interacting mass and momentum equations and membrane transport and concentration polarization models. There are eight membrane elements in the pressure vessel of the RO1 system and seven membrane elements in the pressure vessel of the RO2 system. The water flux in the RO unit is calculated based on the following equation:

$$J_{RO} = Aw_{RO}(\Delta P_{RO} - \sigma \Delta \pi_{RO}) \quad (1)$$

where J_{RO} is the water flux in the RO process, Aw_{RO} is the water permeability, ΔP_{RO} is the difference in the applied pressure, σ is the reflection coefficient, and $\Delta \pi_{RO}$ is the difference in the osmotic pressure which is calculated by the next equation:

$$\Delta \pi_{RO} = (\frac{i*R*T}{Mwt})(C_{Fm,RO} - C_{p,RO}) \quad (2)$$

Where, i is the Van't Hoff factor, R is the real gas constant, T is the feed solution temperature, Mwt is the molecular weight of the solute, $C_{Fm,RO}$ is the feed membrane side concentration, and $C_{p,RO}$ is the product concentration. To determine the product concentration, the equation of the concertation polarization is included with the flux of the solute by the SK model [30] in the RO model, and these are described next:

$$\frac{(C_{Fm,RO} - C_{p,RO})}{(C_{F,RO} - C_{p,RO})} = e^{\frac{J_{RO}}{k_{RO}}} \quad (3)$$

Equation (3) represents the film theory's concentration polarization, where $C_{F,RO}$ is the concentration of the feed solution, and k_{RO} is the mass transfer coefficient. Equation (4) represents the flux of the solute by the SK model:

$$\frac{C_{p,RO}}{C_{F,RO}}\left(1 + \left(\frac{\sigma}{1-\sigma}\right)\left(1 - e^{-J_{RO}(1-\sigma)/B_{RO}}\right)\right) = e^{\frac{J_{RO}}{k_{RO}}} \quad (4)$$

Where, B_{RO} is the solute permeability. Darcy's model is used to determine the pressure drop along the spiral wound membrane as the hydraulic pressure could be varied through the length of the membrane as a function of the feed solution flow rate [33]. For simplicity, the pressure and flow rate are taken to average inlet and outlet conditions. Thus, the pressure drop (Pd_{RO}) in the pressure vessel is calculated as follows:

$$Pd_{RO} = L_{RO} * D_F \frac{Q_{F,RO}+Q_{B,RO}}{2} \quad (5)$$

where L_{RO} is the pressure vessel length which is equal to the multiplication of the length of one membrane module (l_{RO}) times the number of the membrane modules in one pressure vessel (M), D_F is Darcy's law constant for the feed solution, $Q_{F,RO}$, and $Q_{B,RO}$ is the flow rate of the feed and brine solutions, respectively. It is presumed that the pressure of the product solution is 1.5 bar, and the pressure drop in the feed and permeate sides is negligible. The difference in the hydraulic pressure across the RO membrane (ΔP_{RO}) is given as follows:

$$\Delta P_{RO} = P_{F,RO} - \frac{Pd_{RO}}{2} - P_{p,RO} \quad (6)$$

where $P_{F,RO}$ is the hydraulic feed pressure, and $P_{p,RO}$ is the product pressure. The mass transfer coefficient (k_{RO}) is calculated by the following correlation with "x_{RO}" and "y_{RO}" are empirical constants:

$$k_{RO} = x_{RO} \left(\frac{Q_{F,RO}+Q_{B,RO}}{2}\right)^{y_{RO}} \quad (7)$$

The product flow rate is calculated from the following equation:

$$Q_{p,RO} = J_{RO} * Am_{RO} * M \quad (8)$$

where Am_{RO} is the RO membrane area and M is the number of the membrane modules in a pressure vessel. The mass balance equations are included in the model too and added below:

$$Q_{F,RO} = Q_{B,RO} + Q_{p,RO} \quad (9)$$

$$Q_{F,RO} * C_{F,RO} = Q_{B,RO} * C_{B,RO} + Q_{p,RO} * C_{p,RO} \quad (10)$$

Where, $C_{B,RO}$ is the brine solution concentration. The last equation of the RO model is the one of the recovery rate ($Recv_{RO}$), and it is found as follows:

$$Recv_{RO}\% = \frac{Q_{p,RO}}{Q_{F,RO}} * 100\% \quad (11)$$

2.2 The PRO Model

The chosen PRO model in this study is a radial flow model, where feed and draw solutions flow in the radial and axial directions, respectively. The membrane module suggested is a

hollow fibre membrane, where the mathematical model for the HF PRO model is discussed in detail in the literature [34].
The total energy generation (W) and the recovery rate ($Recv_{PRO}$) of the PRO are determined by the next equations [35]:

$$W = \left(Q_{Do,PRO} * P_{Do,PRO}\right) - \left(Q_{Di,PRO} * P_{Di,PRO}\right) \quad (12)$$

$$Recv_{PRO} = \frac{Q_{Do,PRO} - Q_{Di,PRO}}{Q_{Do,PRO}} * 100\% \quad (13)$$

Where, $Q_{Do,PRO}$, and $Q_{Di,PRO}$ is the outlet and the inlet draw flow rate of the PRO unit, respectively, and $P_{Do,PRO}$, and $P_{Di,PRO}$ is the outlet and inlet draw stream pressure of the PRO unit, respectively.

2.3 The Pump Model

The pumps were used in the models for pumping the feed seawater to the RO unit at a fixed pressure. The mass balance of the pump is given below:

$$Q_{Pump,i} = Q_{Pump,o} \quad (14)$$

Where, $Q_{Pump,i,}$ and $Q_{Pump,o}$ are the inlet and outlet flow rates, respectively. The next equation is the momentum balance of the pump:

$$P_{Pump,o} = P_{Pump,i} + P_{Pump,H} \quad (15)$$

where $P_{Pump,o}$, $P_{Pump,i}$, $P_{Pump,H}$ are the outlet, inlet, and head pressures, respectively. The energy consumed by the pump ($W_{Pump,Consumed}$) is determined as follows:

$$W_{Pump,Consumed} = \frac{Q_{Pump,i} * P_{Pump,H}}{\eta_{Pump}} \quad (16)$$

Where, η_{Pump} is the pump efficiency.

2.4 The Energy Recovery Device (ERD) Model

Two streams are entering the ERD, the high-pressure one and the low-pressure one, as shown in Fig. 2. The high-pressure stream will leave the device at lower pressure (P_{ho}) compared to its inlet pressure (P_{hi}), while the low-pressure stream will leave at higher pressure (P_{lo}) compared to its inlet pressure (P_{li}). The mass balance equations in the ERD are given below:

$$Q_{ho} - Q_{hi} = Q_{li} - Q_{lo} \quad (17)$$

$$Q_{li}C_{li} + Q_{hi}C_{hi} = Q_{lo}C_{lo} + Q_{ho}C_{ho} \quad (18)$$

Where, Q_{hi}, Q_{ho}, Q_{li}, and Q_{lo} are the inlet flow rate of the high-pressure stream, the high-pressure outlet stream, the low-pressure inlet stream, and the low-pressure outlet stream, respectively, C_{hi}, C_{ho}, C_{li}, and C_{lo} is the concentration of the high-pressure inlet stream (brine inlet), of the high-pressure outlet stream (feed outlet), of the low-pressure inlet stream (feed inlet), and the low-pressure outlet stream (brine outlet), respectively.

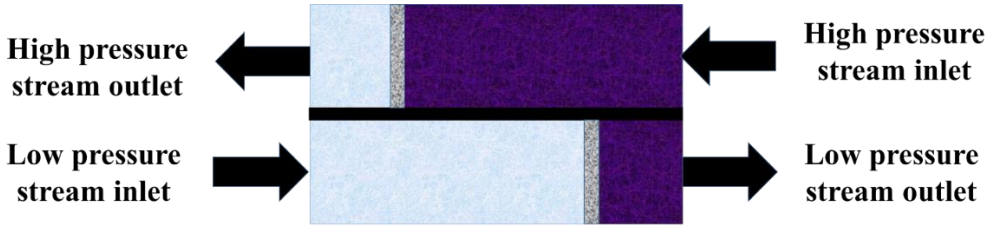

Fig. 2: Representative figure of energy recovery device.

Through the mixing of the two streams of different pressures in the ERD, the outlet concentrations of these streams will vary accordingly and can be estimated by defining the mixing percentage ($\%Mix_{ERD}$) in the ERD as the following:

$$\%Mix_{ERD} = \frac{C_{lo}-C_{li}}{C_{hi}-C_{ho}} * 100\% \quad (19)$$

The following equation is used to calculate the outlet pressure of the low-pressure stream (P_{lo}) based on Bernoulli's equation [36]:

$$P_{lo} = \frac{\eta_{ERD}(Q_{hi}P_{hi}-Q_{ho}P_{ho})+Q_{li}P_{li}-K_{FL}(\eta_{ERD}Q_{ho}\rho_{water}(\frac{Q_{hi}}{A_{ERD}}^2)-Q_{lo}\rho_{water}(\frac{Q_{li}}{A_{ERD}}^2))}{Q_{lo}} \quad (20)$$

where, η_{ERD} is the ERD efficiency, P_{hi}, P_{ho}, P_{li}, and P_{lo} are the pressure of the high-pressure inlet stream, the pressure of the high-pressure outlet stream, and the pressure of the low-pressure inlet stream. In the low-pressure outlet stream, ρ_{water} is the density of the feed water, K_{FL} is the friction loss coefficient, and A_{ERD} is the inlet's side cross-sectional area of the energy recovery device. Next is the lubricant flow (Lub_{flow}) equation in the ERD as a small amount of the high-pressure stream will flow towards the low-pressure stream:

$$Lub_{flow} = Lub_{flowRatio} * Q_{hi} \quad (21)$$

$Lub_{flowRatio}$ is the ratio of the lubricant flow and the inlet flow of the high-pressure stream.

2.5 The Mixer and The Splitter Models

The mixer is used to mix the multiple streams, while the splitter divides one stream into multiple streams. The pressure drop in both models is suggested to be neglected for simplicity. The mass balance for both models is given next:

$$\sum_1^e Q_{i,e} = \sum_1^g Q_{o,g} \quad (22)$$

where e and g are the number of inlet and outlet streams in the corresponding model, $Q_{i,e,}$ and $Q_{o,g}$ are each stream's inlet and outlet flow rate in the corresponding system. The outlet concentration of all streams leaving the splitter will equal the concentration of the inlet stream. On the other hand, the concentration of the outlet stream in the mixer will be determined by the solute balance as the following:

$$\sum_1^e Q_{i,e} C_{i,e} = \sum_1^g Q_{o,g} C_{o,g} \quad (23)$$

where $C_{i,e,}$ and $C_{o,g}$ are each stream's inlet and outlet concentration in the corresponding system.

2.6 The Turbine Model

The turbine is utilized to produce the energy from the inlet pressure head. The next equations are the mass balance and the pressure head for the turbine:

$$Q_{Turbine,i} = Q_{Turbine,o} \quad (24)$$

$$P_{Turbine,o} = P_{Turbine,i} - P_{Turbine,H} \quad (25)$$

where $Q_{Turbine,i,}$ and $Q_{Turbine,o}$ are the flow rate of the inlet and the outlet streams of the turbine, $P_{Turbine,i}$, and $P_{Turbine,o}$ are the pressure of the inlet and the outlet streams of the turbine and $P_{Turbine,H}$ is the head pressure used in the turbine to produce the energy ($W_{Turbine}$) which is determined as next:

$$W_{Turbine} = \eta_{Turbine} * Q_{Turbine,i} * P_{Turbine,H} \quad (26)$$

In Equation 26, η_{Turbine} is the turbine efficiency.

2.7 RO-PRO Hybrid System

The performance of S1-C1 (2RO) and S2-C1 (2RO-DSPRO) was carried out at 40 g/L seawater salinity to compare recovery rate, permeate concentration, and the net specific energy consumption (NSEC). In the S1-C1 system, the permeate from the RO1 membrane will form the feed to the RO2 membrane to provide high-quality freshwater (Fig. 3). For the S2-C1 system, the RO1 permeate and brine will be the feed to the RO2 and the draw solution to the PRO1, respectively (Fig. 1). Then, the diluted draw solution from the PRO1 will form the draw solution of the PRO2 system, using a new wastewater feed solution. The performance of S1-C2 (2RO) and S2-C2 (2RO-DSPRO) was also carried out at 45 g/L seawater salinity to compare recovery rate, permeate concentration, and the net specific energy consumption (NSEC) with S1-C1 and S2-C1 systems. The systems' performance was evaluated at recovery rates between 30 and 46% to determine the net specific energy consumption for desalination.

The permeate from the RO1 membrane in the S1-C2 system will form the feed of the RO2 membrane (Fig. 3). For the S2-C2 system, the RO1 permeate and brine will be the feed to the RO2 and the draw solution to the PRO1, respectively (Fig. 1). Then, the diluted PRO1 draw solution will form the inlet draw solution of the PRO2 system, using a new wastewater feed

solution. The seawater feed flow rate to the HPP4 (Fig. 3) in S1-C2 and the HPP3 (Fig. 1) in S2-C2 was fixed at 172.8 m^3/h and 162 m^3/h, respectively.

3. Results and Discussion

Two scenarios are determined in this study i) two-pass reverse osmosis system (2RO) (Fig. 3) and ii) two-pass reverse osmosis-dual stage pressure retarded osmosis system (2RO-DSPRO) (Fig. 1). The first system consists of 2RO units, with one ERD proposed for freshwater production. The 2RO-DSPRO system will produce freshwater and benefit from the energy generation by the DSPRO.

The seawater is pumped by the high-pressure pump (HPP1) and introduced to the ERD in the 2RO system (Fig. 3) as the low-pressure stream inlet, while the RO1 brine will be the high-pressure stream inlet. The energy will be exchanged in the ERD from the RO1 brine to the seawater, which after leaving the ERD, goes to pump HPP3 and mixed with another high-pressure seawater stream. The RO1 feed stream represents the outlet stream of the mixer. The RO1 product stream will be pressurized in the low-pressure pump (LPP) and sent to the RO2 for freshwater production (RO2 product), and the RO2 brine goes to a turbine for energy recovery.

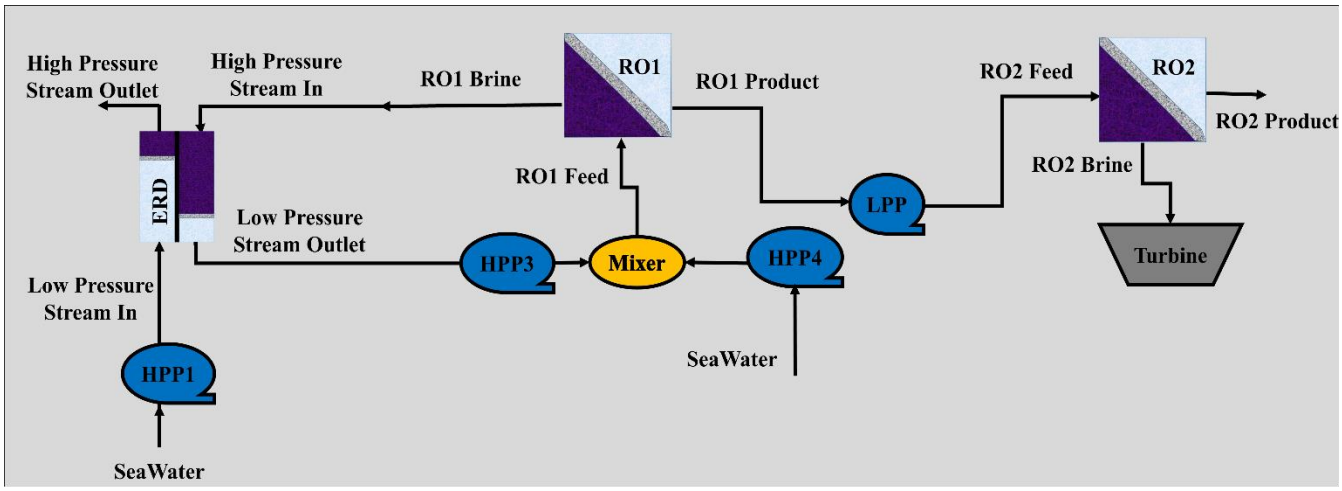

Fig. 3: Schematic diagram of the two-pass RO system for seawater desalination.

The other proposed 2RO-DSPRO hybrid system consists of two RO units (RO1 and RO2) and a DSPRO system (PRO1 and PRO2) (Fig. 1). The system includes three ERDs (ERD1, ERD2, and ERD3) to exchange energy between various streams of different flow rates, concentrations, and pressures. Initially, seawater is pressurized by pump HPP3 and mixed with the low-pressure stream outlet from ERD2 to form the feed stream of the RO1 unit. The RO1 brine stream will be sent to ERD2 to exchange its energy with the low-pressure stream inlet coming from the low-pressure stream outlet from ERD1 (Fig. 1). The high-pressure stream outlet from ERD2 will be the draw solution inlet of the PRO1, in which wastewater solution will be the feed inlet stream. The draw solution outlet of the PRO1 will be sent to ERD1 to exchange energy with the low-pressure seawater inlet of ERD1. In the second DSPRO stage, wastewater is the feed inlet stream, while the high-pressure stream outlet of ERD1 forms the draw solution inlet. Then, the draw outlet stream of PRO2 will go to the ERD3 to exchange energy with the

product stream of the RO1. The low-pressure stream outlet of the ERD3 will be the feed stream of the second RO unit, i.e. RO2, for further treatment and freshwater production.

As shown in Fig. 1 and 3, the main difference between the two systems is the addition of the DSPRO in the second system. The DSPRO will be responsible for energy generation to minimize the net specific energy consumption of the RO plant. The efficiency of HPP, LPP, and ERD is 80%, 80%, and 96%, respectively. Four scenarios of 2RO and 2RO-DSPRO were investigated in this study with 40 g/L and 45 g/L seawater salinities (Table 1). Scenarios S1-C1 and S1-C2 are for the 2RO system without the DSPRO process, and scenarios S2-C1 and S2-C2 with the DSPRO process. The salinity of the feed solution of DSPRO stages one and two was fixed at 1 g/L, while the pressure of the feed solutions was fixed at 1.5 bar, and the feed solution flow rate was fixed at 163 m^3/h. On the other hand, the inlet pressures of the draw solution of the first and second DSPRO stages are fixed at 39 and 26.5 bar, respectively.

Table 1: Type of investigated RO and RO-PRO systems and seawater salinities.

System and Case Number	Abbreviation	RO Units	PRO Units	Seawater Salinity (g/L)
System 1-Case 1	S1-C1	2	-	40
System 2-Case 1	S2-C1	2	2	40
System 1-Case 2	S1-C2	2	-	45
System 2-Case 2	S2-C2	2	2	45

This section will include the RO model validation, the PRO model validation, the comparison of systems net specific energy consumption, the total energy consumed, the total energy generated, the net energy consumed, and the final product concentration.

3.1 The RO and PRO Models Validation

Data from the RO model in Dymola was validated using experimental data of a spiral wound DOW Filmtech (FT-30) RO membrane system [30] of 32 g/L (Table 2). The main parameters of the model as x_{RO}, y_{RO}, Aw_{RO}, B_{RO}, σ, and D_F were determined by using the experimental data to rationalize the model results. Table 2 shows that the absolute percentage error, the difference between the model and the experimental data divided by the experimental data, was between 0.13-10.47 %.

Table 2: The validation results of the RO model.

Feed flow rate (m^3/h)	Feed pressure (bar)	Parameter	Experimental Result	Model Result	Error %
1047.6	50.47	Product Flow Rate (m^3/h)	336.24	351.00	4.39
		Product Concentration (g/L)	0.044	0.0415	5.71
		Brine Pressure (bar)	48.23	49.39	2.40
		Product Flow Rate (m^3/h)	417.60	420.48	0.7

1047.96	55.81	Product Concentration (g/L)	0.049	0.0442	9.79
		Brine Pressure (bar)	54.72	54.79	0.13
1047.96	60.28	Product Flow Rate (m^3/h)	460.80	475.20	3.12
		Product Concentration (g/L)	0.052	0.0466	10.47
		Brine Pressure (bar)	59.22	59.30	0.14

The pilot plant PRO experiments were performed in the Water and Energy Nexus Laboratory, Indian Institute of Technology Guwahati, using a Toyobo hollow fibre (HF) CTA membrane module. The membrane area is 63 $m^{2,}$ and the effective length is 0.78 m. Toyobo membranes can tolerate hydraulic pressure of 30 bar compared to 10 bar for TFC and CTA FO membranes made by Hydration Technology Innovation (HTI, USA) [37]. High pure NaCl purchased from Sigma Aldrich was used to prepare the draw solution with different salinity gradients. The schematic diagram of the experimental setup is shown in Fig. 4. The experimental PRO setup consists mainly of the Toyobo HF PRO membrane module, four tanks for the feed and the draw solutions, a temperature controller for input feed and the draw solutions tank by circulating cold water, and two pumps for pumping the feed and the draw solutions to HF PRO module. The pressure, temperature, flow rate, and volume of the inlet and outlet feed and draw solution were recorded using the data acquisition system (DAS). All the experiments in the current study were performed in counter-current mode, where the feed solution was circulated on the fibre lumen side and the draw solution on the shell side of the HF membrane module. Before the start of the experiment, the feed solution side was closed. Then, the draw solution was circulated in the shell side of the membrane till reaching a steady-state concentration of the draw solutions inlet and outlet, measured by conductivity sensors. The feed solution is passed through the fibre lumen at a constant flow rate by switching on the feed pump VFD. Each experiment was performed three times, and the average of the results was recorded to ensure the accuracy of the results.

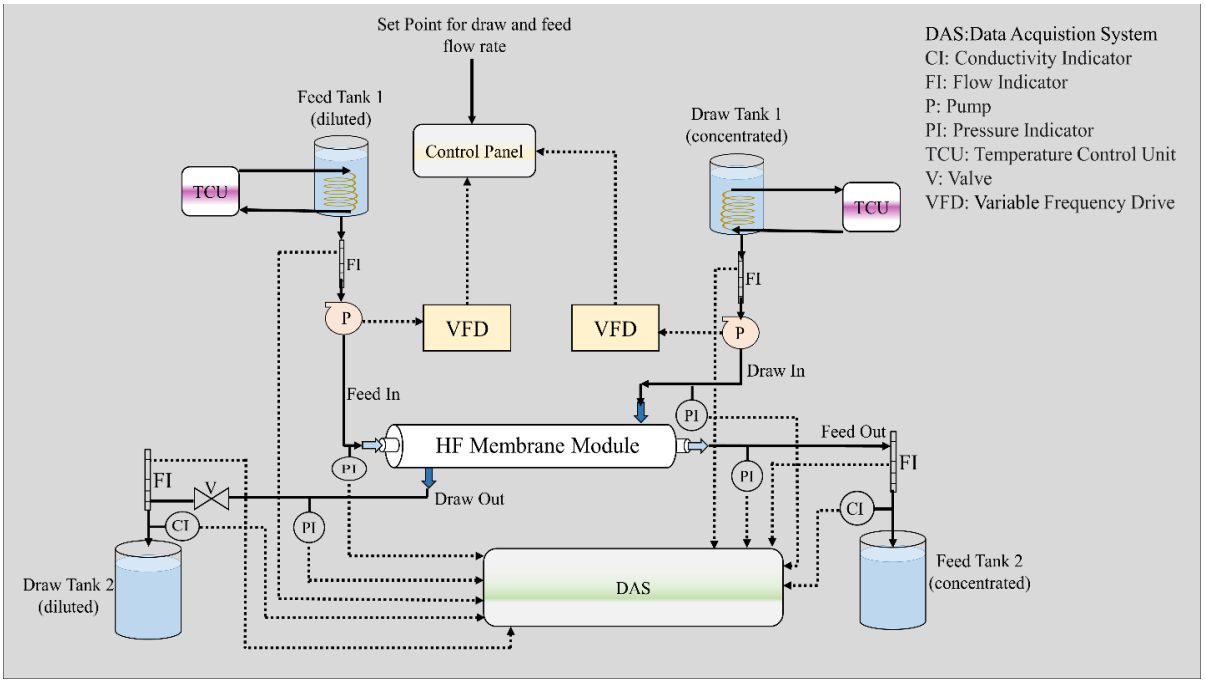

Fig. 4: Schematic diagram of the PRO experimental setup

The PRO plug flow model was validated for a Toyobo HF membrane module (HP5230SI) using Dymola software. The obtained water permeability (A_{WPRO}), the salt permeability coefficient (B_{PRO}), the membrane structural parameter (S_{PRO}), and the mass transfer coefficients for the feed (x_{PRO} and y_{PRO}) of the Toyobo membrane are $1*10^{-7}$ m/bar.s, $6.2*10^{-9}$ m/s, $880*10^{-6}$ m, 0.002068 bar.s/m^4, and 0.501, respectively. The validation results of the PRO model showed a 1.45% to 15% error between the experimental water flux results and the PRO model water flux results (Fig. 5).

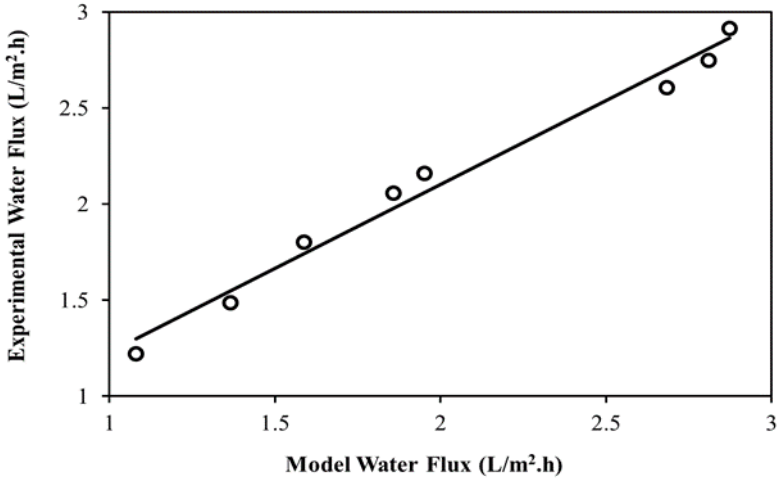

Fig. 5: The model water flux versus the experimental water flux of the PRO system.

3.2 2RO and 2RO-DSPRO Systems of 40 g/L Seawater

The 2RO and 2RO-DSPRO systems' performance was evaluated at recovery rates between 26 and 49%, and the net specific energy consumption was calculated from the following expression:

$$NSEC = \frac{1}{Q_p} * \left(\sum_1^{PN} W_{Pump} - \sum_1^{TN} W_{Turbine}\right) \quad (27)$$

where, NSEC is the net specific energy consumption in kW.h/m^3, *PN* is the number of the pumps in the system, *TN* is the turbines number in the system, W_{Pump} is the consumed energy by the pump in kW, $W_{Turbine}$ is the generated energy by the turbine in kW, and *Qp* is the final product water flow rate in m^3/h.

The seawater feed flow rate to the HPP4 (Fig. 3) in S1-C1 and the HPP3 (Fig. 1) in S2-C1 was fixed at 172.8 m^3/h and 162 m^3/h, respectively. Fig. 6a shows that the RO2 permeate concentration (the final product stream) was higher in S2-C1 compared to S1-C1. The reason for this is that the feed stream of the RO2 unit in S1- C1 represents the product stream of RO1 (Fig. 3), while, in S2-C1, it is the low-pressure stream outlet of ERD 3 (Fig. 1), which is more concentrated than the RO1 product stream in S1-C1. Nevertheless, the final product concentration of both systems shows exceptionally low salinity compared to the allowable drinking water limits (0.25 g/L) [38]. Interestingly, the product concentration of S1-C1 slightly

increased with the RO1 feed pressure due to the recovery rate increase; hence, the bulk concentration of feed solution in the RO1 increased. For the S2-C1, the product concentration decreased with increasing the RO1 feed pressure due to the RO1 feed flow rate increase. As feed pressure increases, the RO1 recovery rate and brine concentration increase, increasing the PRO1 permeation flux and, hence, the ERD1 low-pressure flow rate that composes the feed stream to the RO1 unit (Fig. 1). Moreover, Fig. 6b and Fig. 6c show an increase in the SEC of the RO1 with the increase in the RO recovery rate of S1-C1 and S2-C1 due to the greater feed pressure required to overcome the brine osmotic pressure [30]. The RO1 energy consumption of the S1-C1 and S2-C1 systems is almost the same, while the RO2 energy consumption was higher in the S2-C1 system due to higher feed salinity.

The NSEC of S1-C1 and S2-S1 was calculated for the recovery rates ranging from 26 to 49% by varying the RO feed pressure (Fig. 5d). The NSEC decreased with increasing the feed pressure, then increased again at 66 bar for S1-C1 and 69 bar for S2-C1. However, NSEC was lower in the S2-C1 system than in the S1-C1 system, indicating the role of PRO in reducing desalination energy consumption. For example, at 60 bar, the NSEC of the S2-C1 system was 0.34% lower than that of the S1-C1 system and increased to 15.3% at 74 bar. Similar results were found in the literature [30]. The authors suggested that utilizing a hybrid SWRO-PRO system at 32 g/L draw solution and 1 g/L feed solution saved 16% of the net energy consumption compared to the SWRO system. In general, the profile of NSEC on S1-C1 and S2-C1 agrees with the literature findings that the RO energy consumption reaches an optimum value at a certain recovery rate and then increases due to the increased bulk feed concentration [39]. As shown in Fig 6d, the energy consumption increased at a hydraulic pressure of > 66 bar for the S1-C1 system and at a hydraulic pressure of > 69 bar for the S1-C1 system due to the high energy demand in the RO system.

The RO1 membrane system is practically responsible for the most desalination energy consumption due to high seawater feed salinity (Fig. 6e). In the S1-C1 system, the RO1 was responsible for 93.5 and 89.8% of total energy consumption at 60 and 74 bar feed pressure. The corresponding values for the S2-C1 system are 89.9 and 85.1% of the total energy consumption at 60 and 74 bar feed pressure. In contrast, 6.5 to 10.2% of the total energy consumption was in the RO2 of the S1-C1 system and 10.1 to 14.9% in the RO2 of the S2-C1 system. The difference between the RO1 energy consumption of S1-C1 and S2-C1 systems is 7.4% at 60 bar feed pressure and decreased to 5.2% at 74 bar feed pressure. For the RO2 membrane, the energy consumption in the S1-C1 system was lower than in the S2-C1 system. The RO2 energy consumption of the S2-C1 system was 49% higher than that of the S1-C1 system at 60 bar and 46.4% at 74 bar.

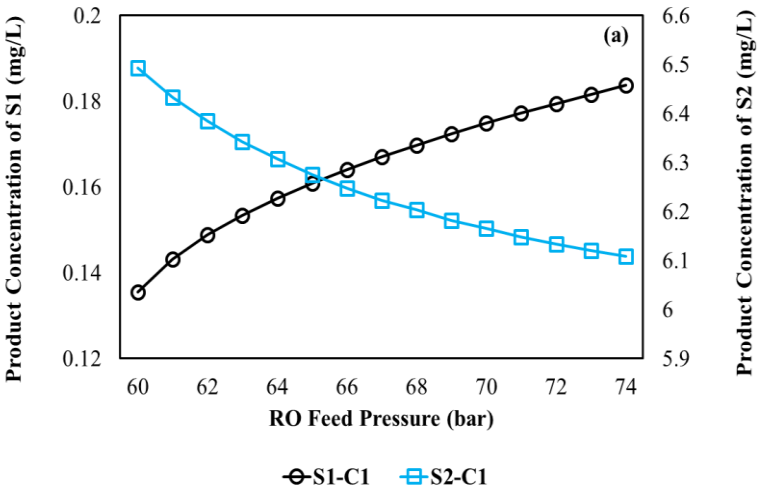
(a)
Product Concentration of S1 (mg/L)
Product Concentration of S2 (mg/L)
0.2
0.18
0.16
0.14
0.12
6.6
6.5
6.4
6.3
6.2
6.1
6
5.9
60
62
64
66
68
70
72
74
RO Feed Pressure (bar)
S1-C1
S2-C1

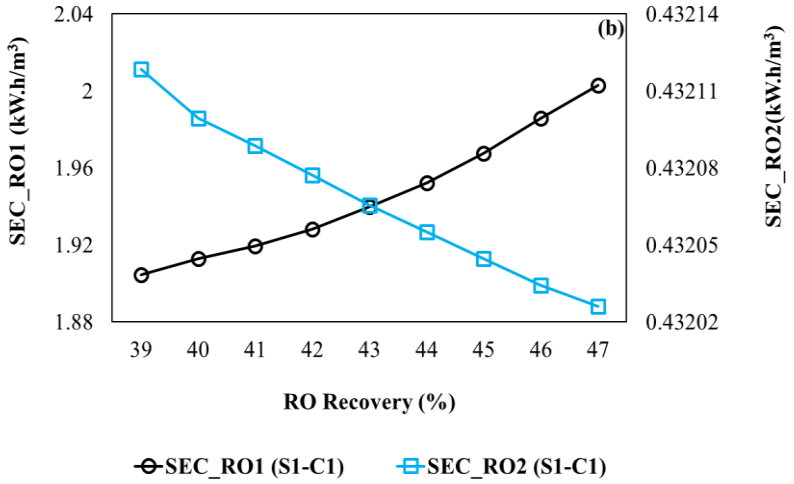
(b)
SEC_RO1 (kW.h/m³)
SEC_RO2(kW.h/m³)
2.04
2
1.96
1.92
1.88
0.43214
0.43211
0.43208
0.43205
0.43202
39
40
41
42
43
44
45
46
47
RO Recovery (%)
SEC_RO1 (S1-C1)
SEC_RO2 (S1-C1)

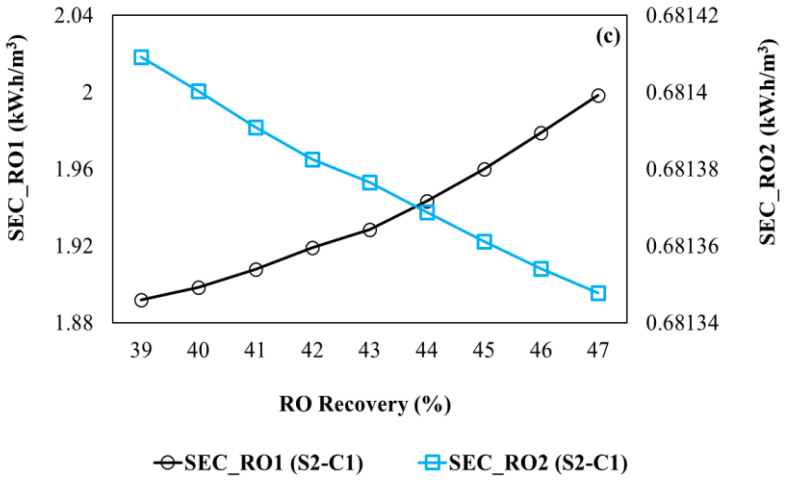
(c)
SEC_RO1 (kW.h/m³)
SEC_RO2 (kW.h/m³)
2.04
2
1.96
1.92
1.88
0.68142
0.6814
0.68138
0.68136
0.68134
39
40
41
42
43
44
45
46
47
RO Recovery (%)
SEC_RO1 (S2-C1)
SEC_RO2 (S2-C1)

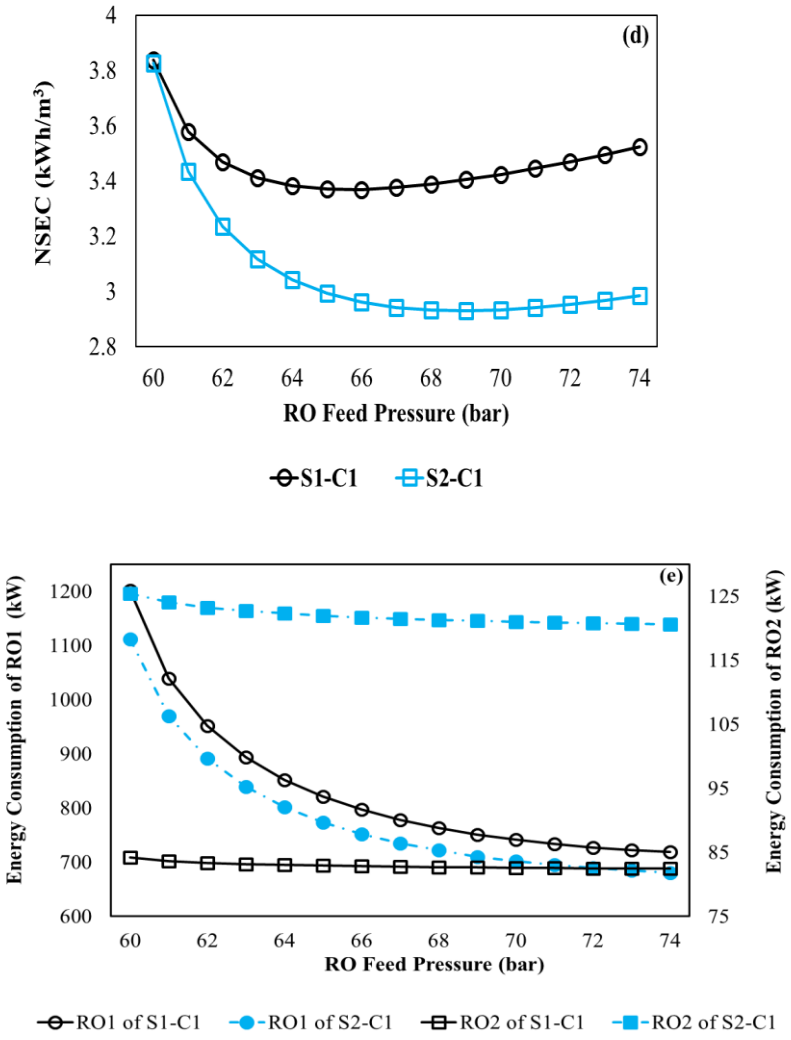

Fig. 6: (a) The product concentration of S1-C1 and S2-C1 with the variation of the RO feed pressure, (b) The SEC of RO1 and RO2 of S1-C1 with the variation of the RO recovery rate, (c) The SEC of RO1 and RO2 of S2-C1 with the variation of the RO recovery rate, (d) The NSEC of S1-C1 and S2-C1 with the variation of the RO feed pressure, (e) The energy consumption of RO1 and RO2 of S1-C1 and S2-C1 with the variation of the RO feed pressure.

Moreover, Fig. 7a displays the energy efficiency of S1-C1 and S2-C1 systems at 39-47% recovery rates. There is an 11.2 to 14.7% decrease in the NSEC of the S2-C1 compared to the S1-C1 system (Fig. 7a). The NSEC of the S1-C1 system increased by increasing the recovery rate from 39 to 47%. In comparison, the NSEC of the S2-C1 system decreased with the recovery rate and reached the lowest value of 2.9 kWh/m^3 at a 45% recovery rate before it increased again. The NSEC of the S1-C1 system at a 45% recovery rate is 3.4 kWh/m^3, which is 14.7% higher than that of the S2-C1 system.

Fig. 7b and 6c show the energy generation and water flux of the DSPRO process in the S2-C1 system. The energy generation of the first PRO stage (PRO1) increased with increasing the recovery rate of the RO system (Fig. 7b) due to the increased water flux (Fig. 7c). Overall, the PRO water flux is directly proportional to the net pressure difference in the PRO [30]. The net pressure difference in PRO2 ($\Delta\pi$-ΔP) has decreased with increasing the recovery rate (Fig. A),

and that causes the drop in the energy generation and the water flux of the PRO2, as shown in Fig. 7b and 7c, respectively.

The maximum energy generation of the PRO1 in the S2-C1 system was 102.7 kW. For the second PRO stage (PRO2) of the DSPRO process, the energy generation decreased with increasing the RO recovery rate (Fig. 7b) due to the decreased water flux (Fig. 7c). The higher energy generation of the PRO2 was 71.9 kW at a 39% recovery rate. The maximum energy generation of the PRO1 is 40.9% higher than that of the PRO2, underlining the fact that PRO1 is responsible for the most energy generated in the DSPRO process.

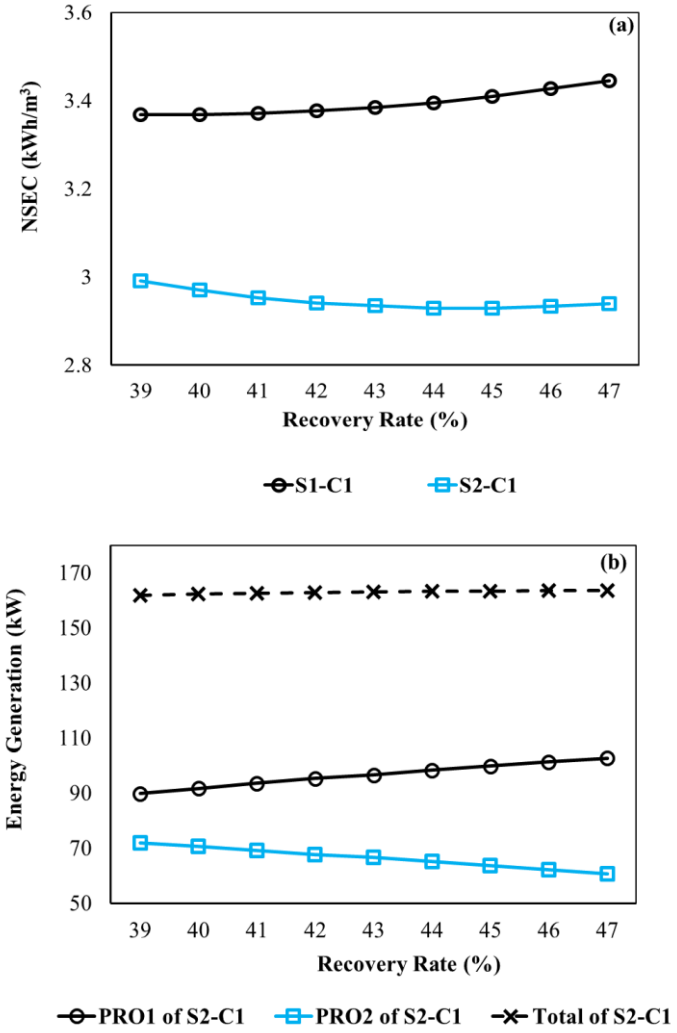

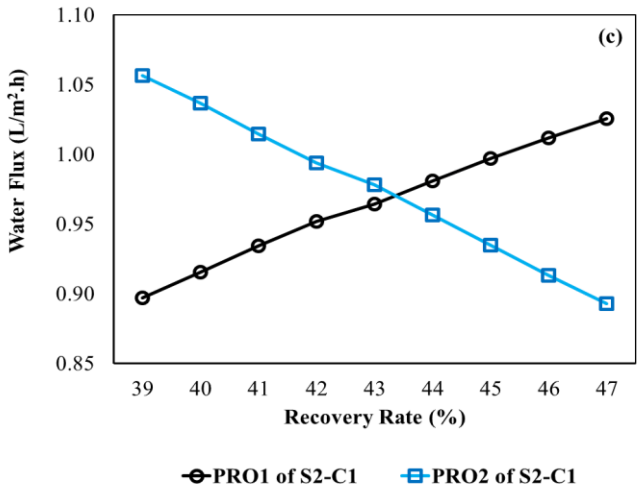

Fig. 7: (a) The NSEC of S1-C1 and S2-C1 with the variation of the recovery rate, (b) The energy generation of PRO1, PRO2, and the total energy generation with the variation of the recovery rate of S2-C1, (c) The water flux of PRO1 and PRO2 with the variation of the recovery rate of S2-C1.

3.3 2RO System and 2RO-DSPRO System of 45 g/L Seawater

The permeate concentration (the RO2 product) was higher in the S2-C2 system than in the S1-C2 system (Fig. 8a). This is because the feed stream of the RO2 unit in the S1-C2 system is the RO1 product (Fig. 3), while it is the low-pressure outlet stream of ERD 3 in the S2-C2 system (Fig. 1). The latter stream is more concentrated than the RO1 product stream in the S2-C2 system. The final product concentration of S1-C2 and S2-C2 systems are much lower than the allowable drinking water limits (0.25 g/L) [38]. Results also showed that the product concentration of the S1-C2 system slightly increased with the RO1 feed pressure due to the recovery rate increase, which in turn increased the bulk concentration of feed solution in the RO1. For the S2-C2 system, the product concentration was reduced with the increase of the RO1 feed pressure due to the increase of the RO1 feed flow rate. As feed pressure increases, the RO1 recovery rate and brine concentration increase, increasing the PRO1 permeation flux and, hence, the ERD1 low-pressure flow rate that forms the feed stream to the RO1 membrane (Fig. 1). Furthermore, Fig. 8b and Fig. 8c show an increase in the SEC of the RO1 with the increase of the RO recovery rate of S1-C2 and S2-C2, respectively [30]. The energy consumption of RO1 was similar in the S1-C2 and S2-C2 systems, but the RO2 energy consumption was higher in the S2-C2 system than in the S1-C2 system due to the higher feed salinity.

The NSEC of S1-C2 and S2-C2 systems was calculated for the recovery rates ranging from 30 to 46% by varying the RO feed pressure (Fig. 8d). The NSEC decreased with increasing the feed pressure, then increased again at 71 bar for the S1-C2 system and 74 bar for the S2-C2 system. However, NSEC was lower in the S2-C2 system than in the S1-C2 system, emphasizing the PRO merit in reducing the desalination energy consumption. For example, at 67 bar, the NSEC of the S2-C2 system was 10.43% lower than that of the S1-C2 system and increased to 17.37% at 77 bar. In general, the profile of NSEC for S1-C2 and S2-C2 systems agrees with the literature findings that the RO energy consumption reaches an optimum value at a certain recovery rate and then increases due to the increased bulk feed concentration [39].

The RO1 membrane system is practically responsible for the most desalination energy consumption due to high seawater feed salinity (Fig. 8e). In the S1-C2 system, the RO1 was responsible for 94.1 and 91.0% of total energy consumption at 67 and 77 bar feed pressure. The corresponding values for the S2-C2 system are 89.1 and 86.5% of the total energy consumption at 67 and 77 bar feed pressure. In contrast, 5.9 to 8.9% of the total energy consumption was in the RO2 of the S1-C2 system and 10.9 to 13.5% in the RO2 of the S2-C2 system. The difference between the RO1 energy consumption of S1-C2 and S2-C2 systems is 24.9% at 67 bar feed pressure and decreased to 7.5% at 77 bar feed pressure. For the RO2 membrane, the energy consumption in the S1-C2 system was lower than in the S2-C2 system. The RO2 energy consumption of the S2-C2 system was 46.7% higher than that of the S1-C2 system at 67 bar and 46.4% at 77 bar.

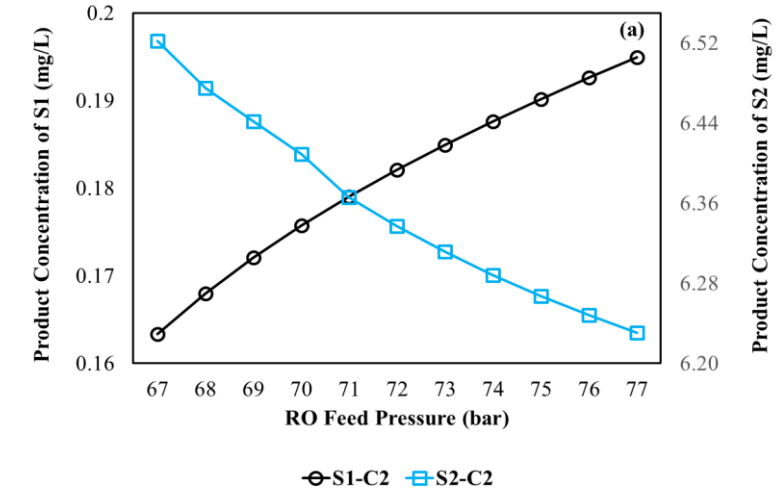

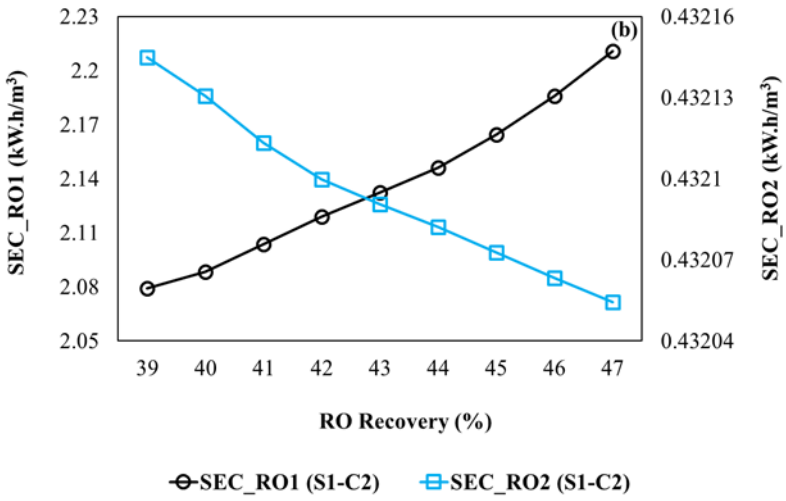

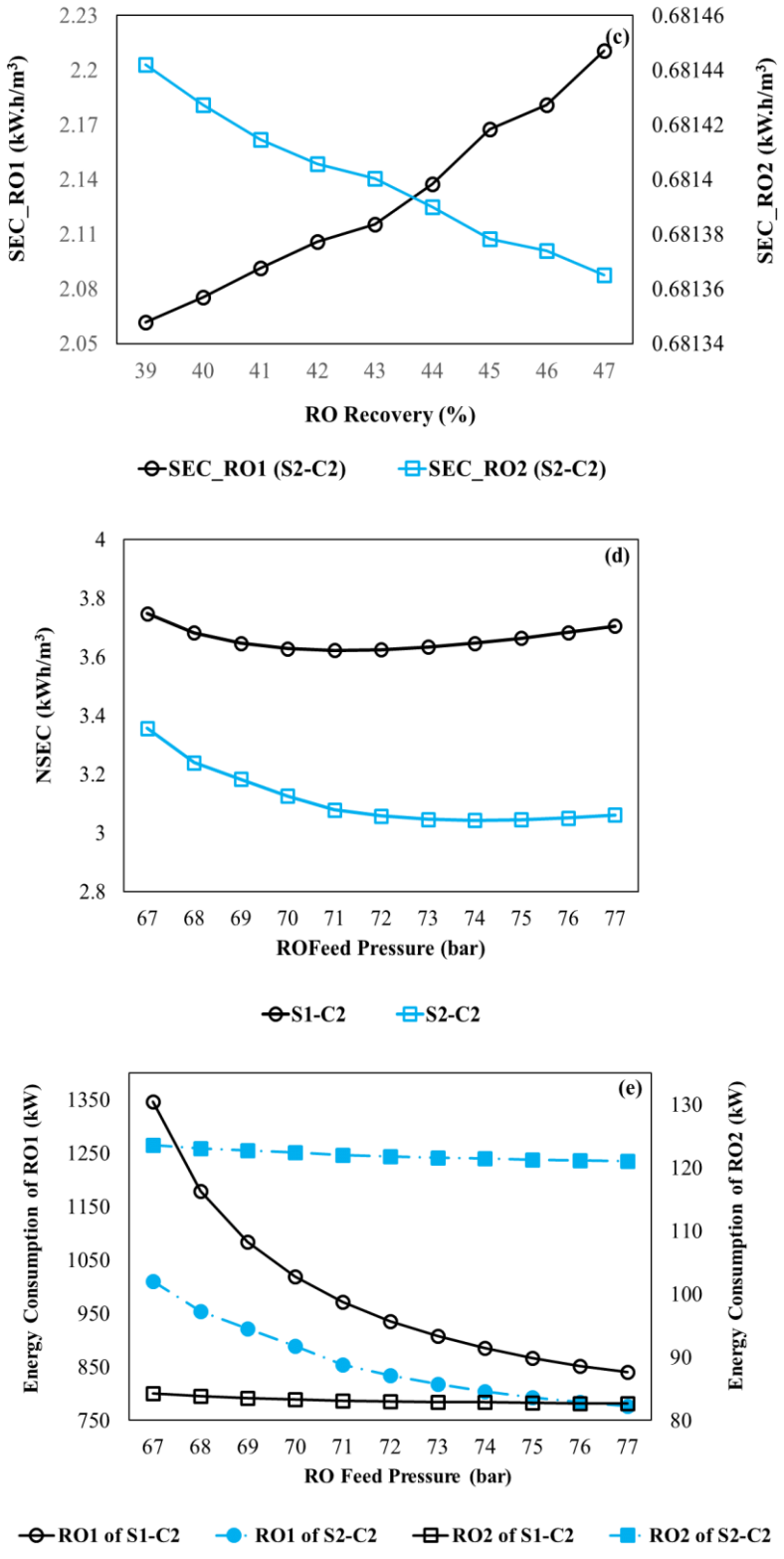

Fig. 8: (a) The product concentration of S1-C2 and S2-C2 with the variation of the RO feed pressure, (b) The SEC of RO1 and RO2 of S1-C2 with the variation of the RO recovery rate, (c) The SEC of RO1 and RO2 of S2-C2 with the variation of the RO recovery rate, (d) The NSEC of S1-C2 and S2-C2 with the variation of the RO feed pressure, (e) The energy consumption of RO1 and RO2 of S1-C2 and S2-C2 with the variation of the RO feed pressure.

Furthermore, Fig. 9a displays the energy efficiency of S1-C2 and S2-C2 systems at 39-47% recovery rates. There is a 15.03 to 17.53% decrease in the NSEC of the S2-C2 compared to the S1-C2 system (Fig. 9a). The NSEC of the S1-C2 system increased by increasing the recovery rate from 39 to 47%. In comparison, the NSEC of the S2-C2 system decreased with the recovery rate and reached the lowest value of 3.04 kWh/m^3 at a 43% recovery rate before it increased again. The NSEC of the S1-C2 system at a 43% recovery rate is 3.7 kWh/m^3, which is 17.8% higher than that of the S2-C2 system.

The energy generation of the DSPRO system was calculated; Fig. 9b and 9c show the energy generation and water flux of the DSPRO process in the S2-C2 system. The energy generation of the PRO1 increased with increasing the recovery rate of the RO system (Fig. 9b) due to the increased PRO1 water flux (Fig. 9c). Overall, the PRO water flux is directly proportional to the net pressure difference in the PRO [30]. The net pressure difference in PRO2 ($\Delta\pi$-ΔP) has decreased with increasing the recovery rate (Fig. A), and that causes the drop in the energy generation and the water flux of the PRO2 (Fig. 9b and 9c).

The maximum energy generation of the PRO1 in the S2-C2 system was 126.7 kW. For the second PRO2 unit, the energy generation decreased with increasing the RO recovery rate (Fig. 9b) due to the decreased water flux (Fig. 9c). The highest energy generation of the PRO2 was 79.3 kW at a 39% recovery rate. The maximum energy generation of the PRO1 is 47.7% higher than that of the PRO2, underlining the fact that PRO1 is responsible for the most energy generated in the DSPRO process.

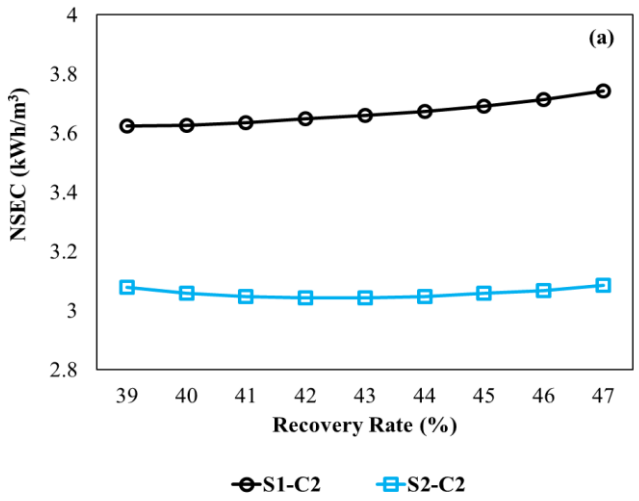

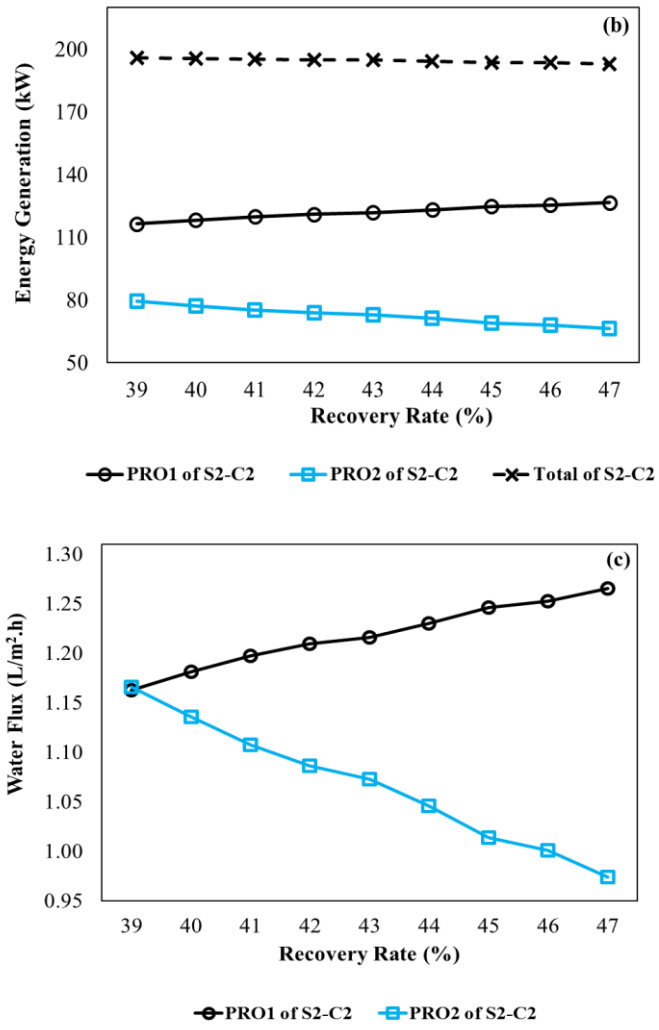

Fig. 9: (a) The NSEC of S1-C2 and S2-C2 with the variation of the recovery rate, (b) The energy generation of PRO1, PRO2 and the total energy generation with the variation of the recovery rate of S2-C2, (c) The water flux of PRO1 and PRO2 with the variation of the recovery rate of S2-C2.

3.4 Comparison between S2-C1 and S2-C2

The performance of the S2-C1 system was compared with that of the S2-C2 system. The difference between the systems is that they use 40 g/L and 45 g/L seawater salinity in the S2-C1 and S2-C2 systems. Fig. 10a shows that the permeate water salinity of the S2-C2 system was greater than that of the S2-C1 system due to the higher seawater salinity. The increase in seawater salinity from 40 g/L in S2-C1 to 45 g/L in the S2-C2 system led to a decrease in the recovery rate of the latter system. For example, at 67 bar feed pressure, the recovery rate was 42% and 31% in the S2-C1 and S2-C2 systems, respectively (Fig. 10b). The NSEC for seawater desalination of the 2RO-DSPRO systems was 2.94 kWh/m^3 for the S2-C1 system and 3.36 kWh/m^3 for the S2-C2 system (Fig. 10c). The higher NSEC in the S2-C2 system is mainly due to the higher energy requirements for desalination in the RO membrane using 45 g/L seawater salinity.

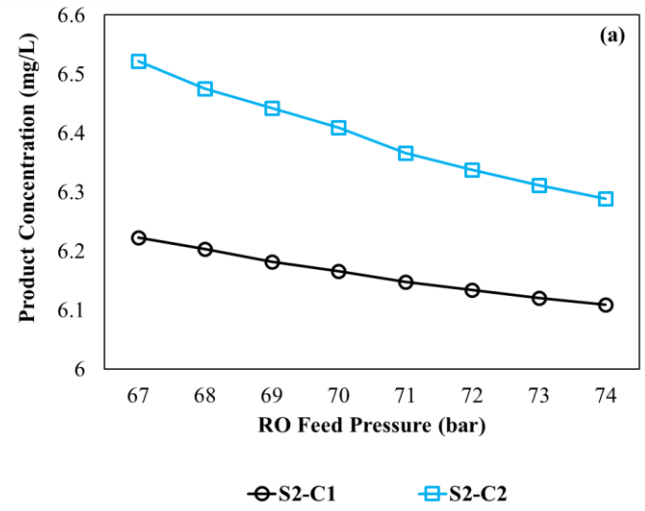
(a)
Product Concentration (mg/L)
6.6
6.5
6.4
6.3
6.2
6.1
6
67
68
69
70
71
72
73
74
RO Feed Pressure (bar)
S2-C1
S2-C2

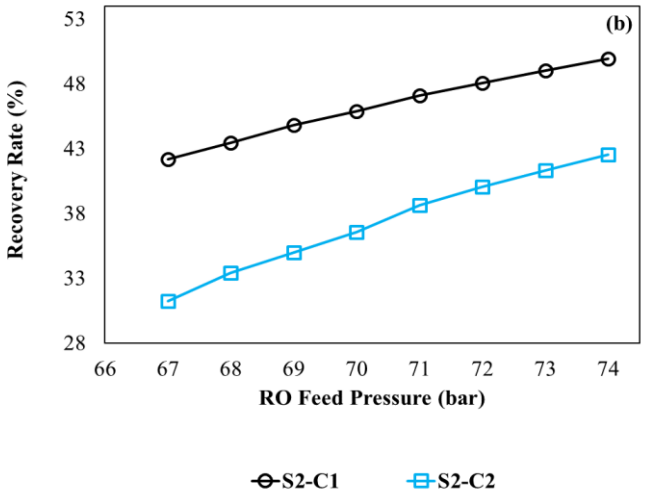
(b)
Recovery Rate (%)
53
48
43
38
33
28
66
67
68
69
70
71
72
73
74
RO Feed Pressure (bar)
S2-C1
S2-C2

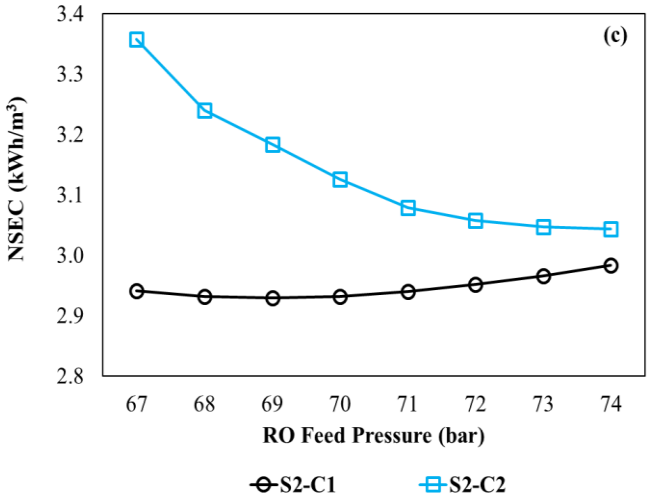
(c)
NSEC (kWh/m3)
3.4
3.3
3.2
3.1
3.0
2.9
2.8
67
68
69
70
71
72
73
74
RO Feed Pressure (bar)
S2-C1
S2-C2

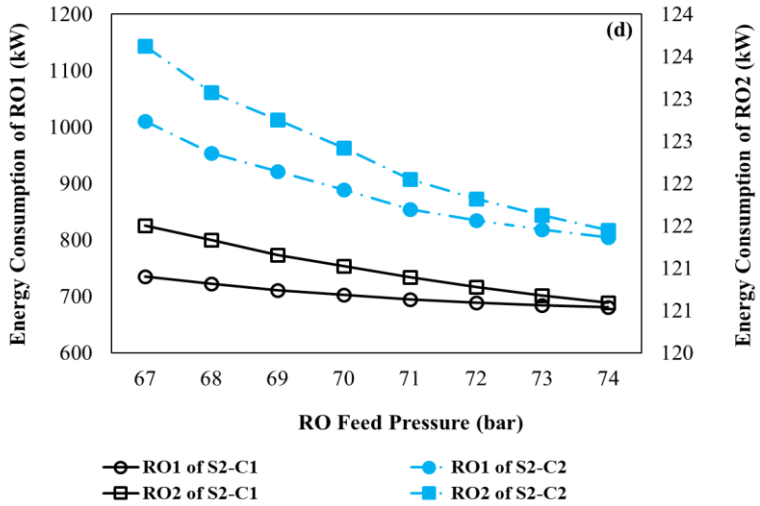

Fig. 10: (a) The product concentration of S2-C1 and S2-C2 with the variation of the RO feed pressure, (b) The recovery rate of S2-C1 and S2-C2 with the variation of the RO feed pressure, (c) The NSEC of S2-C1 and S2-C2 with the variation of the RO feed pressure, (d) The energy consumption of RO1 and RO2 of S2-C1 and S2-C2 with the variation of the RO feed pressure.

Fig. 11a shows the energy generation in the PRO1 and PRO2 of S2-C1 and S2-C2 systems. Results reveal that the energy generation of PRO1 and PRO2 in the S2-C2 system was greater than in the S2-C1 system due to the higher seawater salinity that generated more concentrated brine. The more concentrated brine in the S2-C2 system increased the osmotic pressure gradient in the PRO1 and PRO2, increasing the water flux and energy generation in the DSPRO system (Equation 12). As shown in Fig. 11b, the osmotic pressure difference in the PRO1 and PRO2 of the S2-C2 system was higher than that of the S2-C1 system. The total desalination energy consumption is equal to the energy consumption in the RO1 and RO2 membranes. In contrast, the net energy consumption is determined as the difference between the total energy consumption and the total energy generation in the PRO1 and PRO2 systems. Despite the higher energy generation in the S2-C2 system, Fig. 11d shows that the net energy consumption was higher in the S2-C2 system than in the S2-C1 system. This is attributed to the higher seawater salinity in the S2-C2 system.

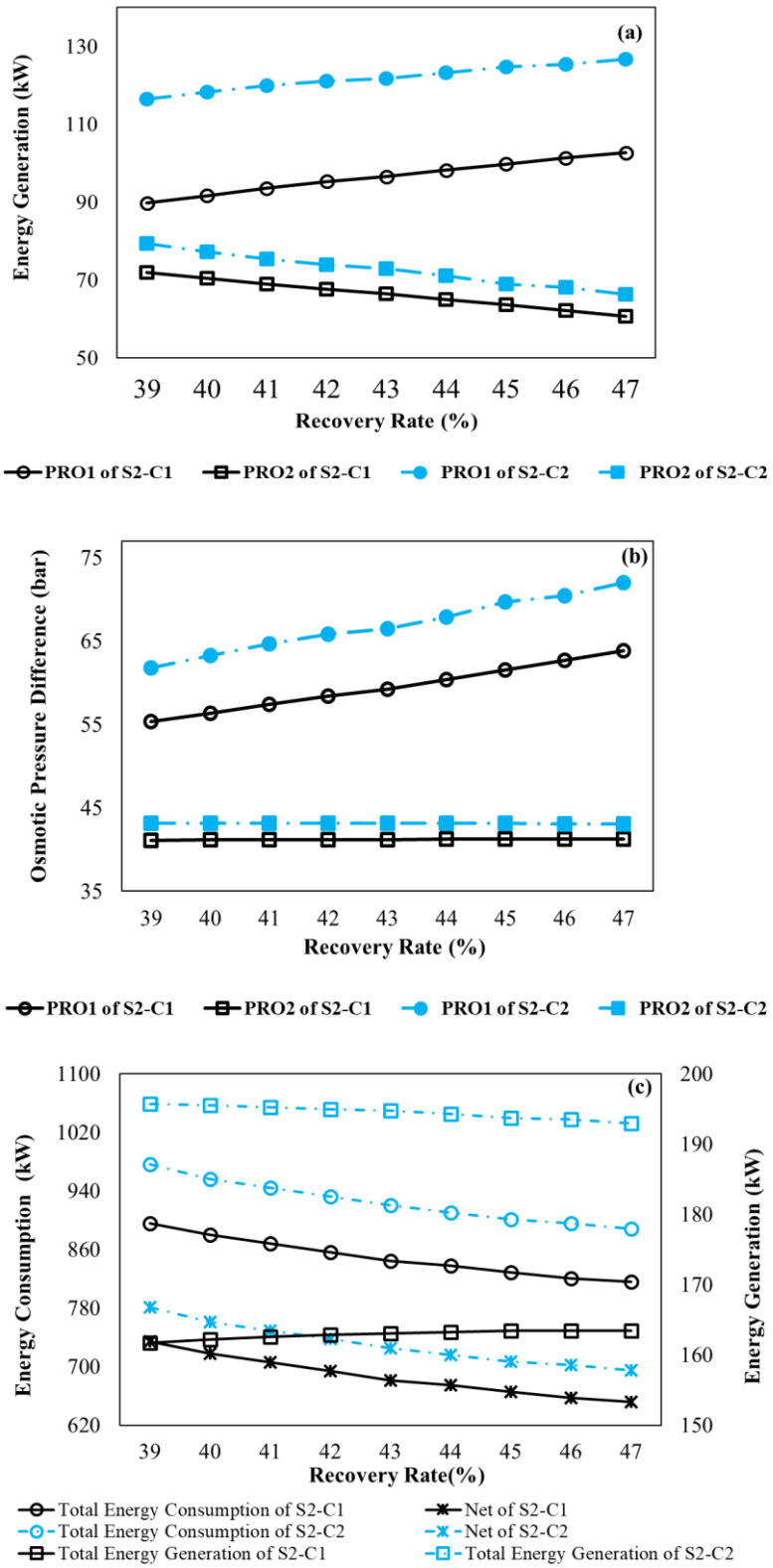

Fig. 11: (a) The energy generation of the PRO1 and PRO2 of S2-C1 and S2-C2 at various recovery rates, (b) The osmotic pressure difference of the PRO1 and PRO2 of S2-C1 and S2-C2 at various recovery rates, (c) The total energy consumption, the total energy generation and the net energy consumption of S2-C1 and S2-C2 at various recovery rates.

3.5 Optimization Problem Formulation

The NSEC is optimized using the "Modelica" modelling language for 158.4 m^3/h capacity two-pass RO desalination plants with and without PRO systems. The main constraints were decided prior to the simulation of the hybrid systems, where parameters that showed a strong impact on the NSEC were selected as the constraints in the optimization problem formulation of the hybrid systems, such as feed and draw solutions flow rate, draw solution pressure, and seawater flow rate[25]. The systems constraints (ranges of the output parameters) and the tuner parameters (input parameters) are illustrated in Table 3, knowing that the tunning parameters related to the PRO system are not applicable for the standalone 2RO plant.

In the case of 40 g/L and 45 g/L seawater TDS, S2-C1 and S2-C2 systems, respectively, the outlet stream of the LPP is sent to ERD3 (Fig. 1), and the other inlet stream to the ERD3 is the draw outlet from the PRO2. The optimization process will change the pressure of the draw solution outlet in the PRO2. Dymola software suggests that the ERD model should fix the pressure of one of the inlet streams; hence, the pressure of the outlet stream of the LPP was fixed in this study. Accordingly, this stream is not included in the optimization problem formulation (Table 3).

Table 3: Constrains and tuner parameters for the 2RO and 2RO-DSPRO systems at 40 g/L and 45 g/L seawater salinity.

Constrains	**S1-C1**	**S2-C1**	**S1-C2**	**S2-C2**
Minimized constrain	NSEC	NSEC	NSEC	NSEC
Equality constrain	$Q_{p,RO2} = 158.4$ (m^3/h)	$Q_{p,RO2} = 158.4$ (m^3/h)	$Q_{p,RO2} = 158.4$ (m^3/h)	$Q_{p,RO2} = 158.4$ (m^3/h)
Inequality constraints	$Recv_{RO1} \leq 45$	$Recv_{RO1} \leq 45$	$Recv_{RO1} \leq 45$	$Recv_{RO1} \leq 45$
		$Recv_{RO2} \leq 95$		$Recv_{RO2} \leq 95$
		$Recv_{PRO1} \leq 45$		$Recv_{PRO1} \leq 45$
	$Recv_{RO2} \leq 95$	$Recv_{PRO2} \leq 45$	$Recv_{RO2} \leq 95$	$Recv_{PRO2} \leq 45$
		$\frac{Q_{Di,PRO1}}{Q_{Fi,PRO1}} \leq 2$		$\frac{Q_{Di,PRO1}}{Q_{Fi,PRO1}} \leq 2$
		$\frac{Q_{Di,PRO2}}{Q_{Fi,PRO2}} \leq 2$		$\frac{Q_{Di,PRO2}}{Q_{Fi,PRO2}} \leq 2$
Tuner Parameter	**S1-C1**	**S2-C1**	**S1-C2**	**S2-C2**
Seawater flow rate	$72 \leq Q_{SW} \leq 324$ (m^3/h)	$72 \leq Q_{SW} \leq 324$ (m^3/h)	$72 \leq Q_{SW} \leq 324$ (m^3/h)	$72 \leq Q_{SW} \leq 324$ (m^3/h)
Pressure of the LPP	$10 \leq P_{LPP} \leq 22$ (bar)	N/A	$10 \leq P_{LPP} \leq 22$ (bar)	N/A
Pressure of the HPP3	$45 \leq P_{HPP3} \leq 85$ (bar)	$45 \leq P_{HPP3} \leq 85$ (bar)	$45 \leq P_{HPP3} \leq 85$ (bar)	$45 \leq P_{HPP3} \leq 85$ (bar)

Feed inlet flow rate of PRO1	N/A	$72 \leq Q_{Fi,PRO1} \leq 324$ (m^3/h)	N/A	$72 \leq Q_{Fi,PRO1} \leq 324$ (m^3/h)
Feed inlet flow rate of PRO2	N/A	$72 \leq Q_{Fi,PRO2} \leq 324$ (m^3/h)	N/A	$72 \leq Q_{Fi,PRO2} \leq 324$ (m^3/h)

After defining the main constraints and the tuner parameters, the optimum NSEC for S1-C1, S2-C1, S1-C2, and S2-C2 systems are determined (Table 4). Fig. 12 shows that the NSEC for the optimized S1-C1, S2-C1, S1-C2, and S2-C2 systems is lower than that for the unoptimized systems. There is a difference between 2.68% and 3.59% in the NSEC in favour of the optimized S1-C1, S2-C1, S1-C2, and S2-C2 systems. The maximum NSEC difference is 3.59% for the S1-C2 system, while the minimum difference is 2.68% for the S2-C1system. The optimum NSEC of S1-C1and S2-C1 systems are 3.25% and 2.91 kWh/m^3, respectively (Table 4). At 40 g/L seawater salinity, the energy-saving due to the optimization of the 2RO-DSPRO hybrid system is 10.46% higher than that of the 2RO system. In contrast, the optimum NSEC of S1-C2 and S2-C2 are 3.49 and 2.97 kWh/m^3 (Table 4). The results indicate that at 45 g/L seawater salinity, the energy-saving due to the optimization of the 2RO-DSPRO hybrid system is 14.92% higher than that of the 2RO system. The increase in energy-saving in the 2RO-DSPRO hybrid systems has highlighted the significance of coupling the DSPRO with the RO plant to reduce desalination energy consumption.

It is noteworthy that the PRO performance is a function of the osmotic pressure gradient of the salinity gradient resource; the higher the osmotic pressure difference, the higher energy extracted in the PRO process. Using the same wastewater feed solution, power generation in the PRO1 and PRO2 from 40 g/L seawater was lower than that from PRO1 and PRO2 from 45 g/L (Fig. 11a). Generally, for the same feed solution concentration, power generation in the PRO process increases with the concentration of the seawater. Therefore, the power generation will be lower at 35 g/L seawater than at 40 g/L and 45 g/L seawater salinity.

Table 4: The NSEC for the optimized 2RO and 2RO-DSPRO systems at 40 g/L and 45 g/L seawater salinity.

Results	**S1-C1**	**S2-C1**	**S1-C2**	**S2-C2**
NSEC	3.25 (kWh/m^3)	2.91 (kWh/m^3)	3.49 (kWh/m^3)	2.97 (kWh/m^3)
Product flow rate	158.4 (m^3/h)	158.36 (m^3/h)	158.4 (m^3/h)	158.47 (m^3/h)
Recovery Rate	$Recv_{RO1}$ = 40%	$Recv_{RO1}$ = 43%	$Recv_{RO1}$ = 39%	$Recv_{RO1}$ = 42%
		$Recv_{RO2}$ = 93%		$Recv_{RO2}$ = 94%
		$Recv_{PRO1}$ = 29%		$Recv_{PRO1}$ = 35%
		$Recv_{PRO2}$ = 30%		$Recv_{PRO2}$ = 31%

	$Recv_{RO2}$ =95%	$\frac{Q_{Di,PRO1}}{Q_{Fi,PRO1}} = 1.3$ $\frac{Q_{Di,PRO2}}{Q_{Fi,PRO2}} = 0.86$	$Recv_{RO2}$ = 95%	$\frac{Q_{Di,PRO1}}{Q_{Fi,PRO1}} = 0.73$ $\frac{Q_{Di,PRO2}}{Q_{Fi,PRO2}} = 0.74$
Tuner Parameter	**S1-C1**	**S2-C1**	**S1-C2**	**S2-C2**
Seawater flow rate	164.16 (m^3/h)	162.60 (m^3/h)	164.12 (m^3/h)	162.68 (m^3/h)
Pressure of the LPP	17 (bar)	N/A	17 (bar)	N/A
Pressure of the HPP3	65 (bar)	67 (bar)	71 (bar)	73 (bar)
Feed inlet flow rate of PRO1	N/A	172.44 (m^3/h)	N/A	313.20(m^3/h)
Feed inlet flow rate of PRO2	N/A	252.04 (m^3/h)	N/A	309.60 (m^3/h)

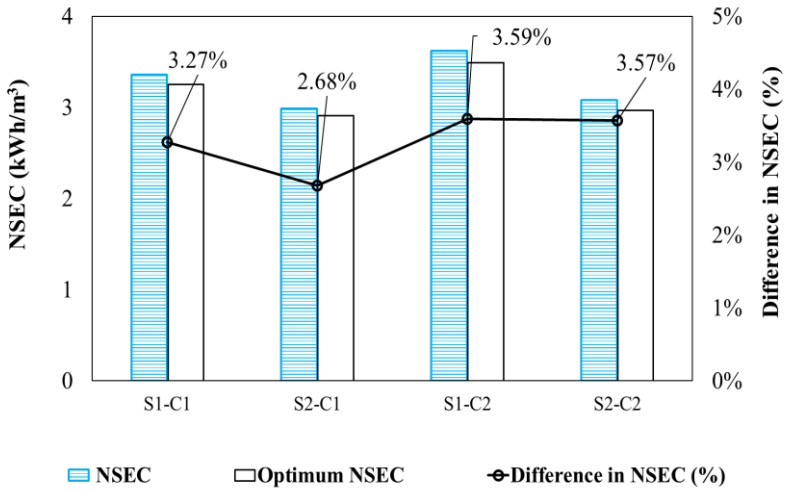

Fig. 12: The NSEC, the optimum NSEC, and the percentage difference in the NSEC of S1-C1, S2-C1, S1-C2, and S2-C2.

3.6 Membrane and Energy Costs

The cost and area of the hollow fibre PRO element in stages one and two were provided by Toyobo Company (Japan), and the spiral wound RO element in stages one and two from the literature [30]. The active membrane and cost of the PRO element are 63 m^2 and $ 5193 US/element, i.e. $ 82 US/m^2. The RO element has 30.5 m^2 of active membrane area and $ 600

US/element, $ 15 US/m^2. The membrane area and cost for two-stage RO and two-stage RO-DSPRO plants of 3801.6 m^3/d capacity were calculated (Table 5). It is worth noting that the reported cost of PRO membranes is the retail cost, and it is expected that this cost will be reduced with increased demand and supply of PRO membranes. The membrane cost is reported based on the retail price for the 70 m^2 PRO membrane model, even though the 650 m^2 PRO model is less expensive. However, the PRO membrane cost is expected to drop in the future or when there is a large market for the PRO technology.

The cost of RO1 in S2-C1 and S2-C2 systems is 5% more expensive than in S1-C1 and S1-C2 systems. The same trend is noticed for RO2, where the cost of RO2 in S2-C1 and S2-C2 systems is 10% more expensive than in S1-C1 and S1-C2 systems due to the higher salinity of feed solution in the former systems, which requires the higher salinity of feed solution larger membrane areas. The required PRO1 membrane area for the S2-C1 system was 23% higher than that for the S2-C2 system due to the higher draw solution concentration in the S2-C2 system using 45 g/L seawater salinity. The higher seawater salinity increased the osmotic pressure of the PRO1 draw solution and the water flux, reducing the required PRO membrane. Similarly, the required PRO2 membrane area for the S2-C1 system was 9% higher than that for the S2-C2. The cost of S2-C1 and S2-C2 systems with PRO units for energy generation is higher than the S1-C1 and S1-C2 systems with RO units only. Toyobo hollow fibre PRO membranes are modified from the RO membrane with a water permeability coefficient of about 0.36 L/m^2h.bar, which is less than the TFC membranes with a water permeability coefficient of about 1.25 L/m^2h.bar [40]. The PRO membrane cost could be reduced by i) applying an improved PRO membrane with a higher water permeability coefficient and ii) reducing the cost of the PRO membrane when there is a big market for the technology. For example, the cots of the PRO membrane could be decreased 6 times when buying a large hollow fibre PRO membrane module.

However, the NSEC of the 2RO-DSPRO system is lower than that of the 2RO system. The NSEC in the S2-C1 system was 9.55% lower than that of the S1-C1 system. For 45 g/L seawater salinity, the NSEC of the S2-C2 was 15% lower than that of the S1-C2 system. The annual energy saving in the 2RO-DSPRO systems S2-C1 and S2-C2 is 471779 and 721544 kWh per year, respectively. 53% more energy-saving was achieved for 45 g/L seawater salinity because of the higher RO brine salinity, underlining that the 2RO-DSPRO system generates more energy than seawater salinity increases.

Table 5: The membrane cost of RO and PRO processes based on the current study.

Process	**Parameter**	**System type**			
		S1-C1	**S2-C1**	**S1-C 2**	**S2-C2**
RO1	Membrane Area (m^2)	5943	6240	5941	6237
	Cost (US$)	89,145	93,600	89,115	93,555
RO2	Membrane Area (m^2)	5813	6419	5819	6429
	Cost (US$)	87,195	96,285	87,285	96,435

PRO1	Membrane Area (m^2)	-	176624	-	136215
	Cost (US$)	-	14,483,168	-	11,169,630
PRO2	Membrane Area (m^2)	-	149914	-	135841
	Cost (US$)	-	12,292,948	-	11,138,962
Total NSEC	kWh/m^3	3.25	2.91	3.49	2.97
Energy Saving	kWh/year		471779		721544
Total cost	($US)	176,340	26,966,001	176,400	22,498,582

Conclusion

The study evaluated the feasibility of coupling the DSPRO with a two-pass RO plant, 2RO-DSPRO, for 40 g/L and 45 g/L salinity seawater treatment. The performance of the 2RO plant was compared with that of the 2RO-DSPRO plant to study the impact of system hybridization on the permeate quality and NSEC. The study showed that 2RO systems provided a higher quality desalinated water than the 2RO-DSPRO system. However, both systems could generate desalinated water that meets the drinking water quality of TDS < 0.25 g/L. The advantage of coupling DSPRO with the 2RO plant was evidenced in reducing the NSEC of the desalination process. At 40 g/L seawater and recovery rates between 39% and 47%, the NSEC of the S2-C1 system was 11.2%-14.7% lower than that of the S1-C1 system (RO plant only).

Interestingly, the reduction in the NSEC of desalination further increased at 45 g/L seawater salinity. At 45 g/L seawater salinity, the NSEC of the S2-C2 system was 15.03%-17.53% lower than that of the S1-C2 system. Furthermore, the optimization of the NSEC showed preferred minimization results. For instance, the NSEC of S1-C2 decreased from 3.62 kWh/m^3 to 3.49 kWh/m^3 after the optimization. The energy generated by the DSPRO will cover part of the energy required for powering the 2RO system, reducing the reliance on fossil fuels and the environmental impact of the CO2 gas emissions. Another significant benefit of the 2RO-DSPRO system is that it would reduce the RO brine concentration due to dilution in the PRO process. Consequently, this will reduce the negative environmental impact of the high concentrated brine on the sea. It should be noted that the cost of the 2RO-DSPRO was around $US 27 million compared to $US176 thousand for the 2RO plant, mainly due to the cost of the PRO membrane. However, the cost of the PRO membrane is expected to decrease when there is a market for the technology.

One of the main obstacles in commercializing the PRO process is finding a suitable membrane and the cost of membranes. Toyobo CTA PRO membrane is about $1.0*10^{-7}$ m/s.bar is rather low compared to $1.69*10^{-7}$ m/s.bar for HTI CTA membrane and $3.25*10^{-7}$ m/s.bar for HTI TFC membrane and $5.25*10^{-7}$ m/s.bar for Porifera TFC membrane. A membrane with higher water permeability is desirable to improve the PRO performance [41]. Also, the cost of the PRO membrane should be affordable, knowing that the Toyobo membrane costs less than HTI and Poreifera membranes [25].

Acknowledgement

The authors wish to express their gratitude for the assistance provided by an Australian Government Research Training Program Scholarship. The RO-PRO pilot plant data used in this project was collected as part of the ongoing technology development project titled "Membrane-based efficient energy storage, clean energy generation, and wastewater treatment system". This project is supported by the Department of Science and Technology, Government of India, Project Number No. DST/TMIWTI/2K16/73 (G).

Appendix A

The Impact of Recovery Rate on the DSPRO Net Pressure Difference

The net pressure difference between the first and the second DSPRO stages is calculated as ($\Delta\pi$-ΔP) and shown in Fig. A concerning the RO1 recovery rate. As shown in the figure, for the PRO2 of the S2-C2 system, there was a sharp drop in the net pressure difference across the membrane with the recovery rate increase. In contrast, for the PRO1 of the S2-C2 system, the net pressure difference across the membranes increased with the recovery rate increase. Technically, the RO brine concentration increases with recovery rates increase, leading to an increase in the osmotic pressure of the PRO1 draw solution. Nevertheless, the PRO2 draw solution is the high-pressure outlet stream of ERD1 (Fig. 1). The concentration of this stream decreases with the increase of the RO recovery rate. Therefore, the net pressure difference of the second DSPRO stage of these two systems decreases with the recovery rate. In general, the concentration of the PRO 1 draw solution is higher at elevated RO1 recovery rates, increasing the performance of the PRO1

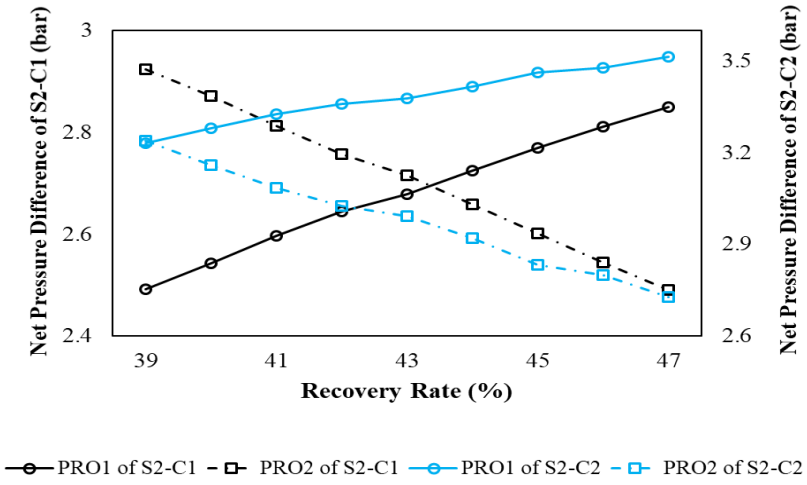

Fig. A: The net pressure difference of the PRO1 and PRO2 of System 2 with the variation of the recovery rate.

References

1. Pan Zhao, et al., *The feasibility survey of an autonomous renewable seawater reverse osmosis system with underwater compressed air energy storage.* Desalination, 2021. **505** DOI: 10.1016/j.desal.2021.114981.
2. C. Lacroix, et al., *Feasibility analysis of a thermo-hydraulic process for reverse osmosis desalination: Experimental approach.* Appl. Therm. Eng., 2022. **213** DOI: 10.1016/j.applthermaleng.2022.118713.
3. Anas Sanna, et al., *Decentralized brackish water reverse osmosis desalination plant based on PV and pumped storage - Technical analysis.* Desalination, 2021. **516** DOI: 10.1016/j.desal.2021.115232.
4. Ruth Kaplan, et al., *Assessment of desalination technologies for treatment of a highly saline brine from a potential CO2 storage site.* DEsalination, 2017. **404**: p. 87-101 DOI: 10.1016/j.desal.2016.11.018.
5. Julian Mamo, et al., *Independent testing of commercially available, high-permeability SWRO membranes for reduced total water cost.* Desalin. Water Treat., 2013. **51**: p. 184-191 DOI: 10.1080/19443994.2012.712242.
6. A. Ruiz-García and I. Nuez, *Simulation-based assessment of safe operating windows and optimization in full-scale seawater reverse osmosis systems.* Desalination, 2022. **533** DOI: 10.1016/j.desal.2022.115768.
7. Tamer M.Mansour, et al., *Energy recovery system in small reverse osmosis desalination plant: Experimental and theoretical investigations.* Alex. Eng. J., 2020. **59**(5) DOI: 10.1016/j.aej.2020.06.030.
8. Maryème Kettani and P. Bandelier, *Techno-economic assessment of solar energy coupling with large-scale desalination plant: The case of Morocco.* Desalination, 2020. **494** DOI: 10.1016/j.desal.2020.114627.
9. S.M. Shalaby, et al., *Reverse osmosis desalination systems powered by solar energy: Preheating techniques and brine disposal challenges – A detailed review.* Energy Convers. Manag., 2022. **251** DOI: 10.1016/j.enconman.2021.114971.
10. Xiaotian Lai, et al., *Solar energy powered high-recovery reverse osmosis for synchronous seawater desalination and energy storage.* Energy Convers. Manag., 2021. **228** DOI: 10.1016/j.enconman.2020.113665.
11. Hamoda Gnaifaid and H. Ozcan, *Development and multiobjective optimization of an integrated flash-binary geothermal power plant with reverse osmosis desalination and absorption refrigeration for multi-generation.* Geothermics, 2021. **89** DOI: 10.1016/j.geothermics.2020.101949.
12. Wuberest Bitew Shumiye, et al., *Exergy analysis of solar-geothermal based power plant integrated with boiling, and reverse osmosis water purification.* Energy Convers. Manag.: X, 2022. **15** DOI: 10.1016/j.ecmx.2022.100255.
13. José A. Carta and P. Cabrera, *Optimal sizing of standalone wind-powered seawater reverse osmosis plants without use of massive energy storage.* Appl. Energy, 2021. **304** DOI: 10.1016/j.apenergy.2021.117888.
14. Carlos Méndez and Y. Bicer, *Integrated system based on solar chimney and wind energy for hybrid desalination via reverse osmosis and multi-stage flash with brine recovery.* Sustain. Energy Technol. Assess., 2021. **44** DOI: 10.1016/j.seta.2021.101080.
15. Katie M. Brodersen, et al., *Direct-drive ocean wave-powered batch reverse osmosis.* Desalination, 2022. **523** DOI: 10.1016/j.desal.2021.115393.
16. Jennifer Leijon, et al., *Variable renewable energy sources for powering reverse osmosis desalination, with a case study of wave powered desalination for Kilifi, Kenya.* Desalination, 2020. **494** DOI: 10.1016/j.desal.2020.114669.

17. Siti Nur Amirah Idris and N. Jullok, *Evaluation of commercial reverse osmosis and forward osmosis membranes at different draw solution concentration in pressure retarded osmosis process.* Mater. Today: Proc., 2021. **46** DOI: 10.1016/j.matpr.2021.03.239.
18. Naomi Sawaki and C.-L. Chen, *Cost evaluation for a two-staged reverse osmosis and pressure retarded osmosis desalination process.* Desalination, 2021. **497** DOI: 10.1016/j.desal.2020.114767.
19. Eleonora Bargiacchi, et al., *Use of Pressure-Retarded-Osmosis to reduce Reverse Osmosis energy consumption by exploiting hypersaline flows.* Energy, 2020. **211** DOI: 10.1016/j.energy.2020.118969.
20. Mohammad Amin Soleimanzade and M. Sadrzadeh, *Deep learning-based energy management of a hybrid photovoltaic-reverse osmosis-pressure retarded osmosis system.* Appl. Energy, 2021. **293** DOI: 10.1016/j.apenergy.2021.116959.
21. Samar AL Mashrafi, et al., *An environmental and economic sustainability assessment of a pressure retarded osmosis system*. Desalination, 2022. **537** DOI: 10.1016/j.desal.2022.115869.
22. Mukesh Sharma, et al., *Clean energy from salinity gradients using pressure retarded osmosis and reverse electrodialysis: A review.* Sustain. Energy Technol. Assess., 2022. **49** DOI: 10.1016/j.seta.2021.101687.
23. Zachary M. Binger and A. Achilli, *Forward osmosis and pressure retarded osmosis process modeling for integration with seawater reverse osmosis desalination.* Desalination, 2020. **491** DOI: 10.1016/j.desal.2020.114583.
24. Qun Wang, et al., *Investigation of the reduced specific energy consumption of the RO-PRO hybrid system based on temperature-enhanced pressure retarded osmosis.* J. Membr. Sci., 2019. **581**: p. 439-452 DOI: 10.1016/j.memsci.2019.03.079.
25. Ali Altaee, Guillermo Zaragoza, and A. Sharif, *Pressure retarded osmosis for power generation and seawater desalination: Performance analysis.* Desalination, 2014. **344**: p. 108–115 DOI: 10.1016/j.desal.2014.03.022.
26. Ali Altaee, Graeme J. Millar, and G. Zaragoza, *Integration and Optimization of Pressure Retarded Osmosis with Reverse Osmosis for Power Generation and High Efficiency Desalination.* Energy, 2016. **103**: p. 110-118 DOI: 10.1016/j.energy.2016.02.116.
27. Wei He, Yang Wang, and M.H. Shaheed, *Stand-alone seawater RO (reverse osmosis) desalination powered by PV (photovoltaic) and PRO (pressure retarded osmosis).* Energy, 2015. **86**: p. 423-435 DOI: 10.1016/j.energy.2015.04.046.
28. Khaled Touati, Fernando Tadeo, and H. Elfil, *Osmotic energy recovery from Reverse Osmosis using two-stage Pressure Retarded Osmosis.* Energy, 2017. **132**: p. 213-224 DOI: 10.1016/j.energy.2017.05.050.
29. MasahideTaniguchi, Masaru Kurihara, and S. Kimura, *Behavior of a reverse osmosis plant adopting a brine conversion two-stage process and its computer simulation.* J. Membr. Sci., 2001. **183**(2): p. 249-257 DOI: 10.1016/S0376-7388(00)00597-4.
30. S. Senthil and S. Senthilmurugan, *Reverse Osmosis–Pressure Retarded Osmosis hybrid system: Modelling, simulation and optimization.* Desalination, 2016. **389**: p. 78-97 DOI: 10.1016/j.desal.2016.01.027.
31. Nahawand AlZainati, et al., *Pressure retarded osmosis: Advancement, challenges and potential.* J. Water Process. Eng., 2021. **40** DOI: 10.1016/j.jwpe.2021.101950.
32. Ali Altaee , et al., *Evaluation the potential and energy efficiency of dual stage pressure retarded osmosis process.* Appl. Energy, 2017. **199**: p. 359–369 DOI: 10.1016/j.apenergy.2017.05.031.

33. Sung-Soo Hong, et al., *Numerical studies on the pressure-retarded osmosis (PRO) system with the spiral wound module for power generation.* Desalin. Water Treat., 2014. **52**: p. 6333-6341 DOI: 10.1080/19443994.2013.821041.
34. Habtom Teklu Aseffa, Dinesh KumarGautam, and SenthilmuruganSubbiah, *Optimization of pressure retarded osmosis process and estimation of Indian blue energy capacity.* Desalination, 2021. **498** DOI: 10.1016/j.desal.2020.114752.
35. Chalida Klaysom, et al., *Forward and pressure retarded osmosis: potential solutions for global challenges in energy and water supply.* Chem. Soc. Rev., 2013. **42**(16): p. 6959-6989 DOI: 10.1039/c3cs60051c.
36. Guirguis, M.J., *Energy Recovery Devices in Seawater Reverse Osmosis Desalination Plants with Emphasis on Efficiency and Economical Analysis of Isobaric versus Centrifugal Devices*. 2011, University of South Florida.
37. Andrea Achilli, Tzahi Y. Cath, and A.E. Childress, *Power generation with pressure retarded osmosis: An experimental and theoretical investigation.* J. Membr. Sci., 2009. **343**(1-2): p. 42-52 DOI: 10.1016/j.memsci.2009.07.006.
38. Lassiter, A., *Rising seas, changing salt lines, and drinking water salinization.* Curr Opin Environ Sustain, 2021. **50**: p. 208-214 DOI: 10.1016/j.cosust.2021.04.009.
39. Adnan Alhathal Alanezi, Ali Altaee, and A.O. Sharif, *The effect of energy recovery device and feed flow rate on the energy efficiency of reverse osmosis process.* Chem. Eng. Res. Des, 2020. **158**: p. 12-23 DOI: 10.1016/j.cherd.2020.03.018.
40. Henrik T. Madsen, et al., *Pressure retarded osmosis from hypersaline solutions: Investigating commercial FO membranes at high pressures.* Desalination, 2017. **420**: p. 183-190 DOI: 10.1016/j.desal.2017.06.028.
41. Machawe M. Motsa and B.B. Mamba, *Forward Osmosis as a Pre-Treatment Step for Seawater Dilution and Wastewater Reclamation*, in *Osmotically Driven Membrane Processes*, Hongbo Du, Audie Thompson, and X. Wang, Editors. 2017.